Generalized coarse-grained Becker–Döring equations

2003 J. Phys. A: Math. Gen. 36 7859

(http://iopscience.iop.org/0305-4470/36/29/301)

INSTITUTE OF PHYSICS PUBLISHING JOURNAL OF PHYSICS A: MATHEMATICAL AND GENERAL

J. Phys. A: Math. Gen. **36** (2003) 7859–7888 PII: S0305-4470(03)59177-6

Generalized coarse-grained Becker–Döring equations

Colin D Bolton and Jonathan A D Wattis

Theoretical Mechanics, School of Mathematical Sciences, University of Nottingham, University Park, Nottingham, NG7 2RD, UK

E-mail: colin.bolton@maths.nottingham.ac.uk and Jonathan.Wattis@nottingham.ac.uk

Received 3 February 2003, in final form 20 May 2003
Published 8 July 2003
Online at stacks.iop.org/JPhysA/36/7859

Abstract

We present and apply a generalized coarse-graining method of reducing the Becker–Döring model; originally formulated to describe the stepwise aggregation and fragmentation of clusters during nucleation. Previous formulations of the coarse-graining procedure have allowed a temporal rescaling of the coarse-grained reaction rates; this is generalized to allow the rescaling to depend on cluster size. The form of this factor is derived for general reaction rates and general mesh function so that the steady-state solution is preserved; in the case of an even mesh function the kinetics can also be accurately reproduced. With a size-dependent mesh function the equilibrium solution and the form of convergence to this state are matched for a specific example. Finally we consider reaction rates relevant to the classical nucleation theory of spherical cluster growth, and numerically compare solutions of the full system to the generalized coarse-grained system in both constant monomer and constant mass formulations, demonstrating the accuracy of the method.

PACS numbers: 05.10.−a, 05.45.−a

1. Introduction

The Becker–Döring [3] model of nucleation is a highly detailed view of nucleation, a consequence of which is a great number of, generally unknown, rate coefficients. Thus the Becker–Döring model relies on the accurate modelling of the numerous rate coefficients, a task which often depends on extrapolating macroscopic data to the microscopic level or vice versa. Additionally the Becker–Döring model contains one equation for each cluster size, a number expected to be vast in general, and this hinders a numerical approach to what initially appears to be a simple scheme of ordinary differential equations. Depending on the growth of the rate coefficients with cluster size, a number of scenarios can be modelled by the system of equations: they can model the formation of polydisperse aggregates which evolve to a steady-state or equilibrium distribution, as well as the case where clusters grow

indefinitely, to arbitrarily large sizes. Recently an approximation to the Becker–Döring model has been proposed to address problems inherent in simulating large systems of this form; the coarse-graining approximation [8, 21]. The aim of this is to reduce the dimensionality of the system and the number of unknown rate coefficients, while retaining the basic structure of the Becker–Döring scheme, hence the features of the model are also preserved at the mesoscopic and ultimately at the macroscopic level. In this paper, we refine the coarse-graining procedure to more accurately describe the kinetics of the system and illustrate it using examples with rate coefficients that are power-law functions of size.

The details of the coarse-graining process have been previously examined in some simple cases. Wattis and King [25] used the example of constant rate coefficients to demonstrate that the coarse-graining procedure should be combined with a temporal transformation and in this simple example a judicious choice of time scaling minimizes errors in the approximation. Additionally Wattis and Coveney have studied the effect of random perturbations to the coarse-graining procedure [24]. In this paper, we generalize the coarse-graining method and investigate a more general definition of coarse-grained rate coefficients to allow the theory to be applied to more complicated aggregation and fragmentation rates. Specifically we allow the coarse-grained reaction rates to be scaled by a size-dependent factor, where as previously this factor was assumed to be size independent.

The coarse-graining approximation has been successfully applied to micelle formation [8], vesicle formation [9] and a generalized nucleation theory incorporating inhibition [21]. In all these examples there is a common approach, that is a microscopic model is developed, and where possible analysed, and then a coarse-graining approximation has been made to simplify the system to allow further analysis of a mesoscopic and macroscopic models.

Such is the rich structure of the Becker–Döring equations that various aspects have been investigated, including the existence of metastable solutions by Penrose [16], the aggregation-dominated regime by Carr and Dunwell [7] and the difficulties in numerically modelling such metastable systems by Carr *et al* [6] and Duncan and Soheili [10]. While being widely applicable the Becker–Döring equations make the restrictive assumption that only monomers may interact with clusters. von Smoluchowski [19] proposed a more general model allowing all cluster sizes to aggregate and for a cluster to split into uneven fragments. Blackman and Marshall [4] exploit the von Smoluchowski equations to study scaling behaviour in essentially the Becker–Döring regime, while Brilliantov and Krapivsky [5] have used a similar approach to study the problem of nucleation with movable monomers and immovable clusters. Additional applications have been transitional aggregation kinetics [13], the origin of the RNA world [22] and monomer–monomer catalysis [12].

The introduction continues with a brief description of the Becker–Döring model and the coarse-graining procedure as previously derived. This section is concluded with the presentation of relevant results for power-law rate coefficients from Wattis and King [11] which will be used in section 3. In section 2 the coarse-graining procedure is generalized for the constant monomer system, by the addition of a size-dependent scaling factor in the coarse-grained rate coefficients, so that the steady-state solutions are faithfully reproduced for completely general rate coefficients and mesh function. This process has one degree of freedom and in section 3 this is exploited in the case of an uniform mesh function (that is the approximation is even over all cluster sizes) to ensure that the kinetics are also matched between the coarse-grained and original system, we use power law rate coefficients with a variety of parameter regimes as examples. In section 4 the case of uneven meshes is investigated and it is concluded that matching the steady-state solution implies that the kinetics will be in error. However, by only matching the equilibrium solution the kinetics can be matched, as shown by a specific example. Duncan and Soheili [10] have numerically compared a variety of methods

for reducing the dimensionality of the Becker–Döring model using rate coefficients relevant to spherical cluster growth; the coarse-graining approximation performed poorly. In section 5 the generalized coarse-graining procedure is applied to the reaction rates used by Duncan and Soheili [10], and we demonstrate that the accuracy is greatly improved compared with previous coarse-graining attempts in both the constant monomer and constant density systems. Finally this paper is concluded by a discussion of the results, given in section 6.

1.1. The Becker–Döring model of nucleation

Becker and Döring [3] presented an enduring model of nucleation in 1935; clusters form by the addition, or subtraction, of single particles (monomers) with no interaction between larger clusters. Such clusters evolve by both monomer aggregation and fragmentation. This process is modelled as a chemical reaction, denoting an r-sized cluster as C_r, we have the reversible reaction

$$C_r + C_1 \rightleftharpoons C_{r+1}. \tag{1}$$

For each reaction there are two reaction rates to prescribe, we denote the forward rate by a_r and the reverse by b_{r+1}, both non-negative. Defining J_r as the net flux from cluster size r to $r+1$ and $c_r(t)$ as the concentration of clusters C_r at time t, we express the system by

$$\dot{c}_1 = 0 \tag{2}$$

$$\dot{c}_r = J_{r-1} - J_r \qquad r \geqslant 2 \tag{3}$$

$$J_r = a_r c_r c_1 - b_{r+1} c_{r+1} \qquad r \geqslant 1 \tag{4}$$

where we assume $\dot{c}_1 = 0$, in the spirit of the original formulation [3]. Later Penrose and Lebowitz [18] generalized these equations by allowing the monomer concentrations to vary; this ensures the conservation of density

$$\rho = \sum_{r=1}^{\infty} r c_r. \tag{5}$$

These modified equations (3)–(5) are still referred to as the Becker–Döring equations. A Lyapunov function exists for the constant monomer Becker–Döring model, namely

$$V(\{c_r\}) = \sum_{r=1}^{\infty} c_r \left(\log\left(\frac{c_r}{Q_r c_1^r} \right) - 1 \right). \tag{6}$$

For certain aggregation and fragmentation rates, the existence and uniqueness of a solution to (2)–(4) have been demonstrated by Ball *et al* [2] for densities below a critical value; furthermore, this result was subsequently generalized to arbitrary initial data by Ball and Carr [1]. The asymptotic solution for size-independent aggregation, and fragmentation, rates has been described by Wattis and King [25]. Our main examples will be taken for the rates $a_r = ar^p$, $b_{r+1} = br^q$, for a variety of choices of p, q, a, b. In section 5 we also consider the case given by $a_r = 1$, $b_{r+1} = Q_r/Q_{r+1}$ with $Q_r = \exp(-(r-1)^{2/3})$. While the Becker–Döring model presents a detailed view of nucleation it can be more insightful to consider a larger scale, mesoscopic, or even a macroscopic representation; an outline derivation of such a theory is presented in the next section.

1.2. Coarse-graining procedure

A coarse-graining procedure for the Becker–Döring model has previously been derived and is summarized here for the constant monomer formulation. The basic idea behind the coarse-graining procedure is to use a mesh function to gather the concentrations into groups of

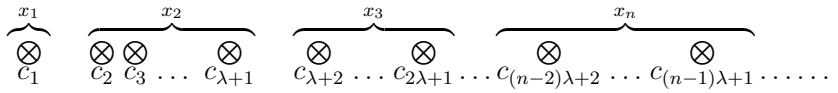

Figure 1. A diagram of the coarse-graining procedure where x_n represents the new co-ordinates and c_r the old concentrations. In this example the number of cluster sizes grouped together to form each x_n is λ, except for the monomer concentration which is represented by x_1. In general λ can be made non-uniform, i.e. $\lambda = \lambda_n$.

consecutive sizes. Each group is represented by the concentration of one particular cluster size in the group. The dynamics of these representative concentrations is governed by a set of coarse-grained equations based on the original Becker–Döring equations. We note that throughout this process the monomer concentration is preserved and kept separate from other clusters due to its unique nature within the Becker–Döring scheme.

To illustrate the method we consider an example where the first λ cluster sizes, after the monomers, are grouped together. Each block of clusters to be grouped together thereafter also contains λ cluster sizes. That is if $\lambda = 2$ then we group together c_2 and c_3 to form x_2, where x_1 has been reserved for the monomer concentration, c_4 and c_5 would then form x_3 etc. The larger the parameter λ, the greater the number of cluster sizes gathered in each group, and the more coarse grained the system is; hence the less microscopic detail that is preserved. We can picture this diagrammatically in figure 1, where in general x_n represents concentrations from $c_{(n-2)\lambda+1}$ to $c_{(n-1)\lambda+1}$. In this scheme we have assumed that the numbers of cluster sizes being assigned to each x_n is the same, with the exception of x_1; however, the theory can easily be generalized to allow this to vary with aggregation number, n, that is x_n contains λ_n concentrations. We define a function, Λ_n, to be the representative cluster size for x_n, that is $x_n = c_{\Lambda_n}$, thus $\lambda_n = \Lambda_{n+1} - \Lambda_n$. In this section we remain with the example where λ is independent of n and so $\Lambda_n = \lambda(n-1)+1$.

We systematically deduce a flux from x_n to x_{n+1}, L_n, by eliminating the concentrations $c_{(n-1)\lambda+2}$ to $c_{n\lambda}$ from the set of microscopic fluxes $J_{(n-1)\lambda+1}, \ldots, J_{n\lambda}$. Then we define $x_n = c_{(n-1)\lambda+1}$ and $x_{n+1} = c_{n\lambda+1}$, that is we set the coarse-grained representative concentration to that of the largest cluster size in the group. Mathematically this choice ensures that when $\lambda = 1$ the original system is recovered. Performing this elimination yields

$$L_n = \alpha_n x_n x_1^{\lambda} - \beta_{n+1} x_{n+1} \tag{7}$$

$$\alpha_n = T(a_{\lambda(n-1)+1} a_{\lambda(n-1)+2} \ldots a_{\lambda n}) \qquad \beta_{n+1} = T(b_{\lambda(n-1)+2} b_{\lambda(n-1)+3} \ldots b_{\lambda n+1}) \tag{8}$$

where T is some associated constant which has previously been assumed to be size independent. In the aggregation term of the flux L_n, the monomer concentration is now raised to a power of λ, which reflects the fact that on average λ monomers are required to aggregate with a cluster to take it from x_n to x_{n+1}. The governing equations for the contracted concentrations, in the case of a constant monomer concentration, are

$$x_1 = c_1 \qquad \dot{x}_n = L_{n-1} - L_n \qquad \forall n \geqslant 2. \tag{9}$$

It is a simple matter to generalize the definitions of L_n (7) and the coarse-grained rate coefficients (8) to the case where the mesh function is size dependent, that is λ depends on n, and so we use the more general definitions

$$L_n = \alpha_n x_n x_1^{\lambda_n} - \beta_{n+1} x_{n+1} \tag{10}$$

$$\alpha_n = T\left(a_{\Lambda_n} a_{\Lambda_n+1} \ldots a_{\Lambda_{n+1}-1}\right) \qquad \beta_{n+1} = T\left(b_{\Lambda_n+1} b_{\Lambda_n+2} \ldots b_{\Lambda_{n+1}}\right). \tag{11}$$

Coveney and Wattis [8] have shown that the coarse-grained system as defined above has the same Becker–Döring structure as the original system; namely (i) there exists a unique equilibrium solution: by setting all the fluxes to zero we obtain

$$\bar{x}_n = Q_{\Lambda_n} x_1^{\Lambda_n} \qquad \frac{Q_{\Lambda_{n+1}}}{Q_{\Lambda_n}} = \frac{\alpha_n}{\beta_{n+1}} \tag{12}$$

(ii) the function

$$V(\{x_n\}) = \sum_{n=1}^{\infty} \lambda_n x_n \left(\log \left(\frac{x_n}{Q_{\Lambda_n} x_1^{\Lambda_n}} \right) - 1 \right) \tag{13}$$

satisfies $\dot{V} < 0$ and qualifies as the Lyapunov function, (iii) there exists the following identities (weak form) for a sequence of numbers $\{h_n\}$

$$\sum_{n=1}^{\infty} h_n \dot{x}_n = \sum_{n=1}^{\infty} (h_{n+1} - h_n - \lambda_n h_1) L_n \tag{14}$$

and finally (iv) if a constant mass system is to be considered there should be one conserved quantity, the density of the coarse-grained system is

$$\rho = x_1 + \sum_{n=2}^{\infty} \lambda_n \Lambda_n x_n \tag{15}$$

where in the summation the λ factor arise because each coarse-grained cluster represents λ original clusters and the Λ_n factor because the coarse-grained concentration x_n represents clusters of size Λ_n. Thus the coarse-grained model has the same structure as the original Becker–Döring system.

Previously Wattis and King [25] noted the need for the parameter T in equation (11) by considering the simple case of size-independent rate coefficients with an even mesh function. With $T = 1$ the steady-state solution was correctly reproduced by the coarse-graining system but the kinetics were incorrect. The solution tends to the steady-state solution via a diffusive wave and it was shown that the correct choice of T matches the speed of this wave in the coarse-grained and original systems. This assumes that T is independent of cluster size; however, if this is the case, then if either the reaction rates or the mesh function λ_n are size dependent, the timescales in the original and coarse-grained system do not agree, and the steady-state solution itself also differs between the original and the coarse-grained systems. In these cases we must allow T to be size dependent (i.e. $T = T_n$) and the determination of such T_n is one of the main themes of this paper. For comparison we use the example of power law rate coefficients recently discussed by King and Wattis [11] and the results used are summarized here.

1.3. Power law rate coefficients

In this section we summarize the results from King and Wattis [11], in which the power law rate coefficients form of the Becker–Döring system, with constant monomer, is solved for a range of parameter regimes. These results will be used for comparison throughout the rest of the paper. The rate coefficients used were $a_r = ar^p$ and $b_r = br^q$ and for these rate coefficients the partition function is given by

$$Q_r = \left(\frac{a}{b}\right)^{r-1} \frac{1}{r^p (r!)^{q-p}}. \tag{16}$$

The equilibrium solution is given by $c_r^{\text{equil}} = Q_r c_1^r$ and if $p < q$ then the partition function converges to zero rapidly enough that the equilibrium distribution is approached; if $q < p$

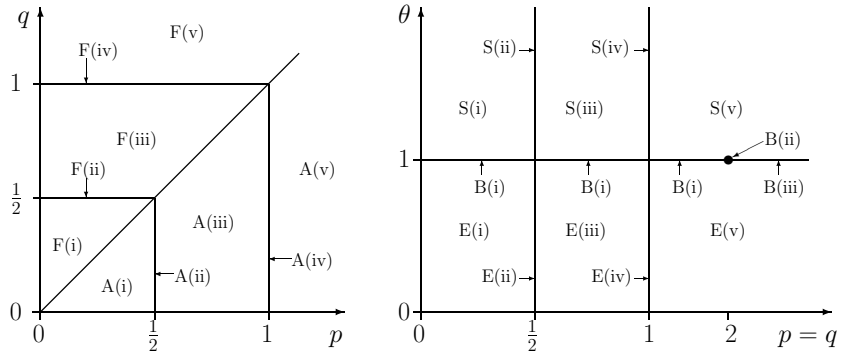

Figure 2. On the left, a diagram of the (p, q) parameter space showing the regions of validity for cases A and F. Cases E, S and B are relevant only when $p = q$, where θ is also relevant for classifying the types of behaviour observed, this is illustrated on the right. Reproduced with permission from the authors [11].

then the large-t asymptotic solution is governed by the approach to a more general steady-state solution, the completely general formula for which is given by

$$c_r^{sss} = Q_r c_1^r \left[1 - J \sum_{k=1}^{r-1} \frac{1}{a_k Q_k c_1^{k+1}} \right] \tag{17}$$

where J is determined by

$$\frac{1}{J} = \sum_{k=1}^{\infty} \frac{1}{a_r Q_r c_1^{r+1}}. \tag{18}$$

In the special case $p = q$ the large-t asymptotic solution depends on $\theta = ac_1/b$; if $\theta \leqslant 1$ then the system converges to the equilibrium solution whilst if $\theta > 1$ a steady-state solution prevails. Figure 2 shows how the regions have been classified by King and Wattis [11], their results for the parameter regions which we will later use as examples are summarized below.

$S(i)$: $p = q < \frac{1}{2}, \theta > 1$. In the case where $p = q < \frac{1}{2}$ and $\theta > 1$ the system converges to the steady-state solution $c_r^{sss} = c_1/r^p$. Defining $\psi(r, t) = c_r(t)\big/c_r^{sss}$, the large time limit of ψ is governed by

$$\frac{\partial \psi}{\partial t} \sim b(1-\theta) r^p \frac{\partial \psi}{\partial r} + \frac{1}{2} b(1+\theta) r^p \frac{\partial^2 \psi}{\partial r^2} \tag{19}$$

whose solution is a travelling and broadening erfc function. To leading order $\psi(r, t)$ is a Heaviside step function with position $s(t)$, given by

$$\dot{s} = (ac_1 - b)s^p \tag{20}$$

and hence $s = (b(\theta - 1)(1 - p)t)^{1/(1-p)}$. Including the next order terms from (19) yield

$$\psi \sim \frac{1}{2} \operatorname{erfc}\left(\sqrt{\frac{(1-2p)(\theta-1)}{2(1+\theta)}} \left(\frac{r - s(t)}{\sqrt{s}} \right) \right). \tag{21}$$

$E(i)$: $p = q < \frac{1}{2}, \theta < 1$. If $p = q$ and $\theta < 1$ then the system converges to the equilibrium solution given by $c_r^{\text{equil}} = \theta^{r-1} c_1 / r^p$. Assuming that $c_r = c_r^{\text{equil}} \psi(r, t)$ it is reported that ψ is an erfc function with position $s(t)$ given by

$$\dot{s}(t) = b(1-\theta)s^p \tag{22}$$

with solution $s = (b(1-\theta)(1-p)t)^{1/(1-p)}$. Using s as an internal time variable, we have

$$\frac{\partial\psi}{\partial s} \sim \frac{1}{2}\frac{1+\theta}{(1-\theta)}\frac{\partial^2\psi}{\partial z^2} - \frac{pz}{s}\frac{\partial\psi}{\partial z} \tag{23}$$

where the transformation $r = s(t) + z$ has been used to render the wave stationary in these co-ordinates. Solving this equation in the large time limit and transforming back to the original co-ordinate yields

$$\psi(r,t) = \frac{1}{2}\operatorname{erfc}\left(\frac{\sqrt{(1-\theta)(1-2p)}}{\sqrt{2(1+\theta)}}\left(\frac{r-s(t)}{\sqrt{s(t)}}\right)\right). \tag{24}$$

$B(i)$: $p = q < \frac{1}{2}, \theta = 1$. The system tends to the equilibrium solution $c_r^{\text{equil}} = c_1/r^p$ and the solution is factored according to $c_r(t) = c_r^{\text{equil}}\psi(r,t)$. The dynamic part, $\psi = \psi(\xi)$, spreads according to the similarity variable $\xi = r/t^{(2-p)}$.

$S(iii)$: $\frac{1}{2} < p = q < 1, \theta > 1$. The system tends towards the steady-state solution but the dynamic part of the solution depends on the initial conditions. In the large time limit the dynamic part will have time dependence of the form $\psi = \psi(\xi)$, with $\xi = (r - s(t))/s^p$, where $\psi(\xi) \longrightarrow 1$ as $\xi \longrightarrow -\infty$ and $\psi(\xi) \longrightarrow 0$ as $\xi \longrightarrow +\infty$. The quantity s is given by $s(t) = (b(\theta-1)(1-p)t)^{1/(1-p)}$ as in S(i).

$A(i)$: $q < p < \frac{1}{2}$. In the parameter regime $q < p < \frac{1}{2}$ the aggregation term dominates fragmentation at large cluster sizes and so the system converges to a steady-state rather than the equilibrium solution. The steady-state solution is derived from equation (17), namely

$$c_r^{sss} = Q_r c_1^r J\sigma(r)$$

with

$$J = \frac{1}{\sigma(1)} \qquad \text{and} \qquad \sigma(r) = \sum_{k=r}^{\infty}\frac{1}{bc_1\theta^k(k!)^{p-q}} \tag{25}$$

with the partition function Q_r given by (16). Factoring the solution according to $c_r = c_r^{sss}\psi(r,t)$ yields the following equation in the limit of large-r,

$$\frac{\partial\psi}{\partial t} \sim -ac_1r^p\frac{\partial\psi}{\partial r} + br^q\frac{\partial\psi}{\partial r} + \frac{ac_1r^p}{2}\frac{\partial^2\psi}{\partial r^2} \tag{26}$$

the solution for large t being given by

$$\psi = \frac{1}{2}\operatorname{erfc}\left(\frac{\sqrt{1-2p}\ (r-s(t))}{\sqrt{2s(t)}}\right) \tag{27}$$

where $s(t)$ is the position of the wave given by

$$\dot{s}(t) = ac_1s^p \tag{28}$$

with solution $s = (ac_1(1-p)t)^{1/(1-p)}$.

$F(i)$: $p < q < \frac{1}{2}$. When $p < q$ the system tends towards the equilibrium solution, $c_r^{\text{equil}} = Q_rc_1^r$, as the fragmentation terms dominate the system for large r. With $c_r(t) = c_r^{\text{equil}}\psi(r,t)$ we find that

$$\frac{\partial\psi}{\partial t} \sim -br^q\frac{\partial\psi}{\partial r} + \frac{1}{2}br^q\frac{\partial^2\psi}{\partial r^2} + b\theta r^p\frac{\partial\psi}{\partial r} \tag{29}$$

and hence in the large-t limit

$$\psi = \frac{1}{2}\operatorname{erfc}\left(\sqrt{\frac{1-2q}{2}}\left(\frac{r-s(t)}{\sqrt{s(t)}}\right)\right) \tag{30}$$

where $s(t)$ is the position of the wave, which to leading order is given by

$$s(t) = (b(1-q)t)^{1/(1-q)}. \tag{31}$$

Having quoted the required results from various parameter regions we consider the generalized coarse-graining system.

2. Generalized coarse-graining procedure

Rather than using the coarse-grained rate coefficients given by (11) we generalize the parameter T by allowing it to depend on the cluster size

$$\alpha_n = T_n\left(a_{\Lambda_n} a_{\Lambda_n+1} \ldots a_{\Lambda_{n+1}-1}\right) \qquad \beta_{n+1} = T_n\left(b_{\Lambda_n+1} b_{\Lambda_n+2} \ldots b_{\Lambda_{n+1}}\right) \tag{32}$$

and we consider the constant monomer formulation of the Becker–Döring model. To determine the size dependence of T_n the steady-state solution, given by (17), between the original and coarse-grained systems is matched; the equilibrium solution is already assured from the structure of definitions (32). The following analysis is valid for all mesh functions Λ_n with the restriction that Λ_n must be monotonically increasing and return only integer values. Firstly, we consider the coarse-grained system; in steady state the flux is constant $L_n = L$ and with equation (7) yields

$$L = T_n x_1^{\Lambda_{n+1}} Q_{\Lambda_{n+1}}\left(b_{\Lambda_n+1} \ldots b_{\Lambda_{n+1}}\right)\left(\frac{x_n}{Q_{\Lambda_n} x_1^{\Lambda_n}} - \frac{x_{n+1}}{Q_{\Lambda_{n+1}} x_1^{\Lambda_{n+1}}}\right). \tag{33}$$

This expression is summed and rearranged to give the steady-state solution for the coarse-grained system, namely

$$x_N = Q_{\Lambda_N} x_1^{\Lambda_N}\left(1 - \sum_{n=1}^{N-1} \frac{L}{T_n x_1^{\Lambda_{n+1}} Q_{\Lambda_{n+1}}\left(b_{\Lambda_n+1} \ldots b_{\Lambda_{n+1}}\right)}\right). \tag{34}$$

To ensure that the steady-state solution for the original and coarse-grained systems match this expression must be compared with equation (17) at the points $r = \Lambda_N$, that is

$$x_N = c_{\Lambda_N}^{sss} = c_1^{\Lambda_N} Q_{\Lambda_N}\left(1 - \sum_{n=1}^{N-1} \sum_{r=\Lambda_n}^{\Lambda_{n+1}-1} \frac{J}{Q_{r+1} c_1^{r+1} b_{r+1}}\right) \tag{35}$$

and so by comparison with equation (34) gives the n-dependence of T_n, namely

$$T_n = \frac{A}{c_1^{\Lambda_{n+1}} Q_{\Lambda_{n+1}}\left(b_{\Lambda_n+1} \ldots b_{\Lambda_{n+1}}\right) \sum_{r=\Lambda_n}^{\Lambda_{n+1}-1}\left(1/Q_{r+1} c_1^{r+1} b_{r+1}\right)} \tag{36}$$

where $A = L/J$, the ratio of the flux in the coarse-grained and original system. Using this general formula for T_n, we are assured that the steady-state and equilibrium solutions will match for completely general reaction rates and mesh functions. Let us consider how the total mass in the full and coarse-grained systems varies over time. For the full system we have

$$\dot{\varrho} = J_1 + \sum_{r=1}^{\infty} J_r \tag{37}$$

where as from (15), for the coarse-grained system, we have

$$\dot{\varrho} = \lambda L_1 + \lambda^2 \sum_{n=1}^{\infty} L_n. \tag{38}$$

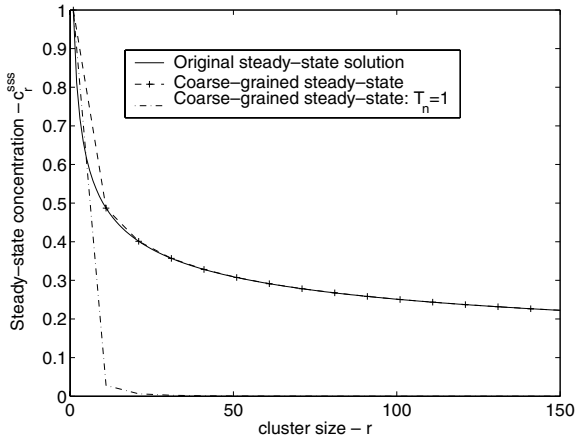

Figure 3. We plot the steady-state concentration against cluster size for the rate coefficients $a_r = ar^p$, $b_r = br^p$ (case S(i)) with parameters $a = 1.6$, $b = 1.4$, $p = 0.3$, $\lambda = 10$ and $c_1 = 1$; the results are plotted at large time, $t = 2000$, when we expect the systems to have reached their respective steady-state solutions. The solid line corresponds to the original system (and confirms that $c_r^{sss} = c_1/r^p$). We then plot the coarse-grained steady-state solution when either $T_n = 1$ $(- - -)$ or T_n as given by equation (39) $(- + -)$, the former does not match with the original system but the latter does to a high degree of accuracy.

If we assume the system is in some state where the steady-state $J_r = J$ (18) is valid for all $r < R \gg 1$ and $c_r \approx 0$ for $r > R$ then $\dot{\varrho} \sim RJ$. In the coarse-grained system we thus have $L_n = L$, for $n < N$ and $x_n = 0$ for $n > N$. Thus in the coarse-grained system we have $\dot{\varrho} = \lambda^2 LN$; comparing this with the result for the full system we have $N\lambda^2 L = RJ$, and since $R = \lambda N$ this can be simplified to $\lambda L = J$, and thus we expect $A = 1/\lambda$; a result we demonstrate in the following examples.

3. Uniform mesh function with power law rate coefficients

Defining T_n by equation (36) the steady-state solution will be reproduced in the coarse-grained system; however, careful choice of the parameter A also allows the kinetics to be matched in many cases. We demonstrate this for a size-independent mesh function and a constant monomer system with power law rate coefficients in the parameter regimes previously discussed in section 1.3.

3.1. Case S(i): $p = q < \frac{1}{2}, \theta > 1$

For the case $p = q < \frac{1}{2}$ and $\theta > 1$ the expression (36) for T_n simplifies to

$$T_n = \frac{A(\theta - 1)}{b^{\lambda-1}(\theta^{\lambda-1})} \frac{(\Lambda_n!)^p}{((\Lambda_{n+1} - 1)!)^p}. \tag{39}$$

This formula gives the required n-dependence for T_n such that the steady state will be reproduced in the coarse-grained system. The result of choosing T_n correctly is shown in figure 3, where parameter values $p = q = 0.3$, $a = 1.6$, $b = 1.4$, $\lambda = 10$ and $c_1 = 1$ have been used. The original steady-state solution, which we are trying to reproduce, is plotted with the coarse-grained system; to compare, we plot the numerical result at large time with $T_n = 1\ \forall n$ and again with T_n as given by (39) with $A = 1$. Clearly with $T_n = 1$ the steady-state

solution is not reproduced accurately ($x_n \sim x_1/n^{p\lambda}$ as $n \longrightarrow \infty$), however, by choosing T_n as above (39) the numerical solutions show perfect agreement ($x_n \sim x_1/(\Lambda n)^p$ as $t \longrightarrow \infty$). Any choice of A reproduces the steady-state solution in the large time limit but with $A = 1$ we find that the coarse-grained system evolves faster than the original system and so we proceed to deduce the correct value of A to match these evolutions.

The steady-state solution is given by $x_n^{sss} = x_1/\Lambda_n^p$, derived from equation (17), and we factorize according to $x_n(t) = x_1\Psi(n,t)/\Lambda_n^p$. We now seek a similar solution for Ψ to that of the original system, that is we expect Ψ to have the form of a diffusive wave. We substitute this form of x_n into the equation for $\dot{x}_n$ as given by (9) to yield

$$\frac{1}{\Lambda_n^p}\frac{\partial\Psi(n,t)}{\partial t} = \frac{A(\theta-1)}{b^{\lambda-1}(\theta^\lambda-1)}\big[a^\lambda x_1^\lambda\Psi(n-1,t) - b^\lambda\Psi(n,t) - a^\lambda x_1^\lambda\Psi(n,t) + b^\lambda\Psi(n+1,t)\big]. \tag{40}$$

We take the limit $n \longrightarrow \infty$; in this limit $\Lambda_n \sim \lambda n$ and a continuum limit for Ψ is appropriate, hence

$$\frac{\partial\Psi}{\partial t} \sim -b(\theta-1)(\lambda n)^p A\frac{\partial\Psi}{\partial n} + \frac{A(\lambda n)^p b(\theta^\lambda+1)(\theta-1)}{2(\theta^\lambda-1)}\frac{\partial^2\Psi}{\partial n^2}. \tag{41}$$

To leading order $\Psi(n,t) = H(\eta(t)-n)$ where upon we deduce that

$$\dot{\eta} = b(\theta-1)\lambda^p\eta^p A. \tag{42}$$

We expect that the speed of the wave front for the original system, $s(t)$, and that of the coarse-grained system $\eta(t)$ will be related by $\dot{s} = \lambda\dot{\eta}$. Thus we relate equations (20) and (42) and deduce that $A = 1/\lambda$. So this choice of A matches the speed of evolution for the original and coarse-grained system in the large n, and hence large time, limit. However, due to differences in the evolution of the original and coarse-grained systems over $\mathcal{O}(1)$ timescales we must allow a time shift to match the positions exactly. Using the parameters $a = 1.7, b = 1.4, c_1 = 1$ and $p = q = 0.4$ we have numerically solved the original and the contracted system, with $\lambda = 10$. We define the position of the diffusive wave by determining where ψ or Ψ equals $\frac{1}{2}$ and plot the results in figure 4, where we have shifted time in the coarse-grained position by +3, and the positions are shown to match perfectly even at moderate times.

To obtain the shape of the function Ψ we convert (41) to the original co-ordinates, that is $r = \Lambda_n$ and $s(t) = \Lambda_\eta$. Further transforming the co-ordinates to a frame of reference where the wave is stationary, that is $r = z + s(t)$ where $\dot{s} = b(\theta-1)s^p$, yields for the contracted system

$$\frac{\partial\Psi}{\partial t} \sim -b(\theta-1)pzs^{p-1}\frac{\partial\Psi}{\partial z} + \frac{b(1+\theta^\lambda)(1-\theta)\lambda s^p}{(1-\theta^\lambda)}\frac{\partial^2\Psi}{\partial z^2}. \tag{43}$$

The required solution to this equation is

$$\Psi = \frac{1}{2}\operatorname{erfc}\left(\frac{\sqrt{(1-2p)(\theta^\lambda-1)}}{\sqrt{2(1+\theta^\lambda)\lambda}}\frac{(r-s(t))}{\sqrt{s}}\right) \tag{44}$$

thus by comparison with equation (4.25) from [11] the ratio of widths in the original (w_s) and coarse-grained (w_c) system in the large time limit is given by

$$\frac{w_o}{w_c} = \frac{\sqrt{(\theta+1)(\theta^\lambda-1)}}{\sqrt{\lambda(\theta^\lambda+1)(\theta-1)}}. \tag{45}$$

Since this ratio is t-independent then it follows that the coarse-grained system achieves the correct exponent of t in the dependence of the width and is in error only by the multiplying

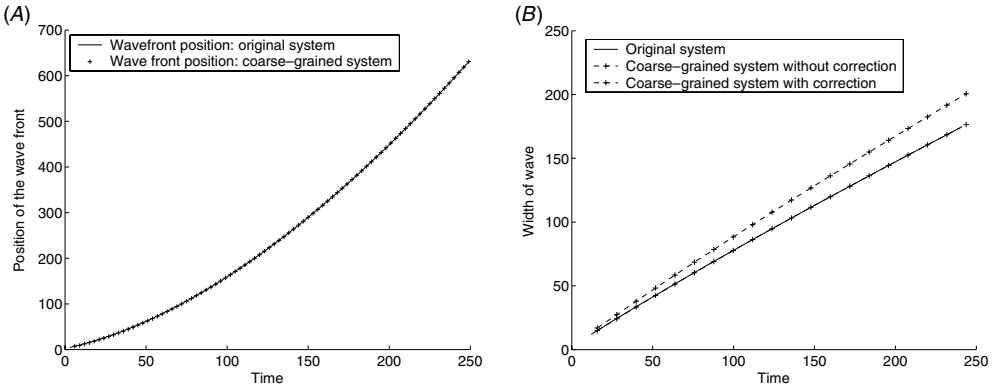

Figure 4. (*A*) A plot of the position of the diffusive wave ($\psi = \frac{1}{2}$) for the original and coarse-grained system with rate coefficients $a_r = ar^p$, $b_r = br^p$ (case S(i)), $a = 1.7, b = 1.4, p = 0.4, \lambda = 10$ and $c_1 = 1$. With a time shift of +3 to the coarse-grained system these positions are found to match exactly. (*B*) Evolution of width of diffusive wave in cluster-size against time. We divide the numerical value of $x_n(t)$ by the steady-state solution x_n^{sss} to obtain $\Psi_n(t)$. We estimate the width of this function by the interquartile range n_+–n_-, where $\Psi_{n_+}(t) = 0.75$ and $\Psi_{n_-}(t) = 0.25$. We plot this width over time for the original and coarse-grained system, and the latter with a scaling factor. We find that the coarse-grained system does not reproduce the width of the original system, but it is in error by only a constant factor predicted by (45).

scalar. Additionally we note that in the limit $\theta \longrightarrow 1$, $(\theta^\lambda - 1)/\lambda(\theta - 1) \longrightarrow 1$ and $(\theta + 1)/(\theta^\lambda + 1) \longrightarrow 1$; so in the limit $\theta \longrightarrow 1$ the width is correctly reproduced by the coarse-grained system. We note that the greatest error in the width is a factor of $1/\sqrt{\lambda}$ in the limit $\theta \longrightarrow \infty$. This result is confirmed numerically with the parameters $a = 1.7, b = 1.4, p = q = 0.4, \lambda = 10$ and $c_1 = 1$. The wave is extracted by dividing the concentrations $c_n(t)$ by the steady-state solution c_r^{sss}, and the width is estimated by the difference between where the wave is equal to $\frac{3}{4}$ and $\frac{1}{4}$. In figure 4 the width between the original and coarse-grained system is compared, firstly we observe that the width in the coarse-grained system is too large and, furthermore, that multiplying the coarse-grained width by the factor w_o/w_c recovers the correct width as required (a time shift of +3.795 has been applied to match large time position $s(t)$).

Thus far an expression for the scaling factors T_n has been deduced which correctly reproduces the steady-state solution in the coarse-grained system, as well as the speed of evolution to this state. We proceed by demonstrating that the choice of T_n (39) also matches the speed of evolution to the equilibrium solution.

3.2. Case E(i): $p = q < \frac{1}{2}, \theta < 1$

For $p = q < \frac{1}{2}$ and $\theta < 1$ the original system tends to the equilibrium solution and we are assured that the coarse-grained system will reproduce the equilibrium solution faithfully; however, we now show that the choice of T_n as given by (39) with $A = 1/\lambda$ also matches the speed of convergence to this state.

We calculate an expression for the speed of convergence to the equilibrium solution for the coarse-grained system. Writing the x_n variables according to $x_n = c_{\Lambda_n}^{\text{equil}}\Psi(n,t) = \theta^{\Lambda_n - 1}x_1\Psi(n,t)\big/\Lambda_n^p$, and substituting this form of x_n into the equation for $\dot{x}_n$ (9) yields

$$\frac{\partial \Psi(n,t)}{\partial t} \sim T_{n-1} b^{\lambda} \frac{(\Lambda_n!)^p}{(\Lambda_{n-1}!)^p} (\Psi(n-1,t) - \Psi(n,t)) + T_n b^{\lambda} \frac{(\Lambda_{n+1}-1!)^p}{(\Lambda_n - 1!)^p} \theta^{\lambda} (\Psi(n+1,t) - \Psi(n,t)). \tag{46}$$

We take the large-n limit, in which $\Lambda_n \sim \lambda n$, this also allows us to take the continuum limit for Ψ and so to leading order

$$\frac{\partial \Psi}{\partial t} = b^{\lambda} \left[T_n \frac{((\Lambda_{n+1}-1)!)^p}{((\Lambda_n - 1!))^p} \theta^{\lambda} - T_{n-1} \frac{(\Lambda_n!)^p}{(\Lambda_{n-1}!)^p} \right] \frac{\partial \Psi}{\partial n}. \tag{47}$$

We note that we have left the factorials unapproximated for ease of comparison later. In the first approximation we take $\Psi(n,t)$ to be the Heaviside step function of the form $\Psi(n,t) = H(\eta(t) - n)$ as previously and so we deduce that

$$\dot{\eta} = -b^{\lambda} \left[T_{\eta} \frac{((\Lambda_{\eta+1}-1)!)^p}{((\Lambda_{\eta} - 1!))^p} \theta^{\lambda} - T_{\eta-1} \frac{(\Lambda_{\eta}!)^p}{(\Lambda_{\eta-1}+1)!)^p} \right]. \tag{48}$$

We require that $\lambda \dot{\eta} = \dot{s}$ and so with (22) we obtain the difference equation

$$\frac{\lambda b (1-\theta) \eta^p}{\lambda^p} = -\lambda b^{\lambda} \left[T_{\eta} \frac{((\Lambda_{\eta+1}-1)!)^p}{((\Lambda_{\eta} - 1)!)^p} \theta^{\lambda} - T_{\eta-1} \frac{(\Lambda_{\eta}!)^p}{((\Lambda_{\eta-1}+1)!)^p} \right]. \tag{49}$$

Substitution confirms that T_n as given by (39) does indeed satisfy this difference equation with $A = 1/\lambda$, as required. So T_n given by (39) gives the correct leading order dynamics for both cases S(i) and E(i) and also the correct form for the steady-state solution. With this expression for T_n, Ψ is governed by

$$\frac{\partial \Psi}{\partial t} \sim -\frac{\Lambda_n^p (1-\theta) b}{\lambda} \frac{\partial \Psi}{\partial n} + \frac{b(1-\theta)(1+\theta^{\lambda}) \Lambda_n^p}{2\lambda(1-\theta^{\lambda})} \frac{\partial^2 \Psi}{\partial n^2}. \tag{50}$$

Performing a similar calculation to that in section 3.1 where the co-ordinates are shifted by $r = z + s(t)$, we find that the function Ψ for the coarse-grained system is given by

$$\Psi = \frac{1}{2} \operatorname{erfc} \left(\frac{\sqrt{(1-2p)(1-\theta^{\lambda})}}{\sqrt{2(1+\theta^{\lambda})\lambda}} \frac{(r - s(t))}{\sqrt{s}} \right) \tag{51}$$

the ratio of the widths in the original (w_o) and coarse-grained (w_c) system is given by

$$\frac{w_o}{w_c} = \frac{\sqrt{(1+\theta)(1-\theta^{\lambda})}}{\sqrt{\lambda(1+\theta^{\lambda})(1-\theta)}} \tag{52}$$

and again we note that in the limit $\theta \longrightarrow 1$ this tends to unity and is bounded above by 1 and below by $1/\sqrt{\lambda}$ (which is approached in the limit $\theta \longrightarrow 0$).

3.3. Case B(i): $p = q < \frac{1}{2}, \theta = 1$

For the case $p = q$, we confirm that the previous analysis is also valid for the border line case B(i) where $\theta = 1$. Numerical simulations were performed, and figure 5 displays results for the case with the parameters $p = q = 0.4, a = b = 1.2$, $c_1 = 1$ and $\lambda = 10$. Firstly we compare the steady state that the coarse-grained and the original system tend to in the long time limit; figure 5(*A*) compares these at $t = 1000$, confirming that the original system tends to the equilibrium solution and additionally that the coarse-grained system tends to this solution also, when T_n is given by

$$T_n = \frac{A}{\lambda b^{\lambda - 1}} \frac{(\Lambda_n!)^p}{((\Lambda_{n+1}-1)!)^p}.$$

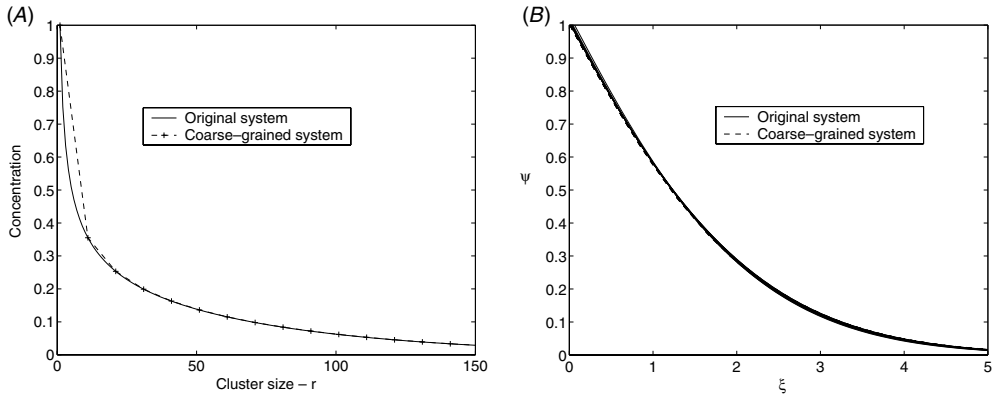

Figure 5. We numerically solve case B(i) with parameters $a = b = 1.2$, $p = q = 0.4$, $\lambda = 10$ and $c_1 = 1$. (*A*) The solution is plotted for $t = 1000$ for both the coarse-grained and original system. Firstly we note that the original system tends to the solution $c_r^{\text{equil}} = 1/r^p$ as stated by [11] and furthermore the coarse-grained system also tends to this state. (*B*) We extract the divide the numerical solution by the equilibrium solution $c_r^{\text{equil}} = 1/r^p$. We plot $\psi = r/t^{2-p}$ against the similarity variable ξ for the original and coarse-grained system for the time range $100 < t < 1000$ in steps of 100. We note that the widths match exactly with a shift of -0.468 applied to the width of the coarse-grained system.

Previously we noted that the original system spreads according to the similarity variable $\xi = r/t^{(2-p)}$ and defining a measure of the width of ψ as the position where $\psi = 0.5$, the width of the coarse-grained and original systems are compared in figure 5. The widths are plotted against ξ over the time range $100 < t < 1000$ in steps of 100; not only do the curves for the original system match but also the coarse-grained system gives the same solution as the full system. Hence the coarse-grained width matches exactly that of the original system, as expected since in the regions S(i) and E(i) it was found that in the limit $\theta \longrightarrow 1$ the widths of the coarse-grained and original system agreed (see (45) and (52)).

3.4. Case S(iii): $\frac{1}{2} < p = q < 1, \theta > 1$

The system with $\frac{1}{2} < p = q < 1$ and $\theta > 1$ is investigated numerically with the coarse-graining parameter T_n as given by (39), calculated in case S(i). Figure 6 shows results for the case with $a = 1.2$, $b = 0.8$, $p = q = 0.6$, $c_1 = 1$ and $\lambda = 10$. The function ψ is plotted for the original system by dividing the numerical solution by the steady-state solution and this is plotted for the time range $12 < t < 140$ in steps of 12. As time progresses the function ψ is plotted against ξ and this tends towards a fixed form determined by the initial conditions, as predicted previously. We expect that the choice of T_n from (39) will match the speed of evolution $s(t)$ in the coarse-grained system to that of the original system, but not the width of the function ψ. We plot the function Ψ over time for the coarse-grained system against the parameter

$$\Xi = \frac{(n-1)\lambda + 1 - s(t)}{s(t)^p} \tag{53}$$

where we convert back to the original co-ordinates using $\Lambda_n = (n-1)\lambda + 1$ but the expression for the speed, s, is expected to be the same due to the correct choice of T_n; the results for $12 < t < 140$ are shown in figure 6. Again as $t \longrightarrow \infty$ the solution tends to a fixed function

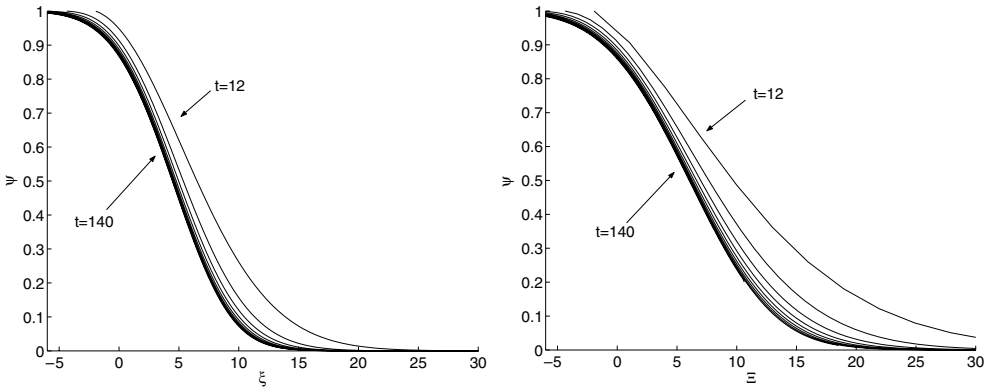

Figure 6. We extract the dynamics by dividing the numerical solution by the equilibrium solution and plot this for the time range $12 < t < 140$ in steps of 12 for the original and coarse-grained system against the parameter ξ or Ξ, respectively, with rate coefficients $a_r = ar^p$, $b_r = br^p$ (case S(iii)) with parameters $a = 1.2, b = 0.8, p = 0.6$ and $c_1 = 1$. We note that as $t \longrightarrow \infty$ the solution tends to a fixed function and that the form of the coarse-grained system is similar to that of the original system, but wider as expected.

which has a similar form to the original system but, as expected, the coarse-grained system has a broader distribution compared with the original system. Numerically the ratio of the widths of the original and coarse-grained system is $w_o/w_c = 7.02$ which is in good agreement with the analytical prediction from equations (45) and (52), namely $w_o/w_c = 6.95$.

3.5. $A(i)$: $q < p < \frac{1}{2}$

If $q < p < \frac{1}{2}$ then the original system (2)–(4) will tend to the steady-state solution (17). We use the form of T_n given by (36) to ensure that the steady state is reproduced faithfully in the coarse-grained system and this form of T_n is verified numerically, with $A = 1$. Using the parameters $a = 1.7, b = 1.4, p = 0.2, q = 0.4, c_1 = 1$ and $\lambda = 10$ we numerically integrate the original and coarse-grained system, comparing the result after sufficient time to allow the systems to reach their steady-state solutions; these are compared in figure 7 and the results match exactly. We proceed by deriving the constant A which regulates the speed of evolution of the coarse-grained system.

The time-dependent part of the solution is factored as previously to give $x_n(t) = c^{sss}_{\Lambda_n}\Psi(n,t) = Q_{\Lambda_n} c_1^{\Lambda_n} J\sigma(\Lambda_n)\Psi(n,t)$ which is substituted into (9), and hence

$$\begin{aligned}\dot{\Psi}(n,t) = {} & \frac{L}{Q_{\Lambda_n} J x_1^{\Lambda_n}\left(\sum_{k=\Lambda_{n-1}}^{\Lambda_n - 1}\left(1/a_k Q_k x_1^{k+1}\right)\right)}(\Psi(n-1,t) - \Psi(n,t)) \\ & + \frac{L}{Q_{\Lambda_n} J x_1^{\Lambda_n}\left(\sum_{k=\Lambda_n}^{\Lambda_{n+1}-1}\left(1/a_k Q_k x_1^{k+1}\right)\right)}(\Psi(n+1,t) - \Psi(n,t)) \\ & + \frac{L}{Q_{\Lambda_n} J x_1^{\Lambda_n}\sigma(\Lambda_n)}(\Psi(n-1,t) - \Psi(n+1,t)). \end{aligned} \tag{54}$$

The limit $n \longrightarrow \infty$ is considered, which allows a continuum approximation to be taken, which to second order is

$$\frac{\partial \Psi}{\partial t} \sim \frac{L}{J}(-a x_1 (\lambda n)^p + b(\lambda n)^q)\frac{\partial \Psi}{\partial n} + \frac{L}{J}\frac{a x_1 (\lambda n)^p}{2}\frac{\partial^2 \Psi}{\partial n^2}. \tag{55}$$

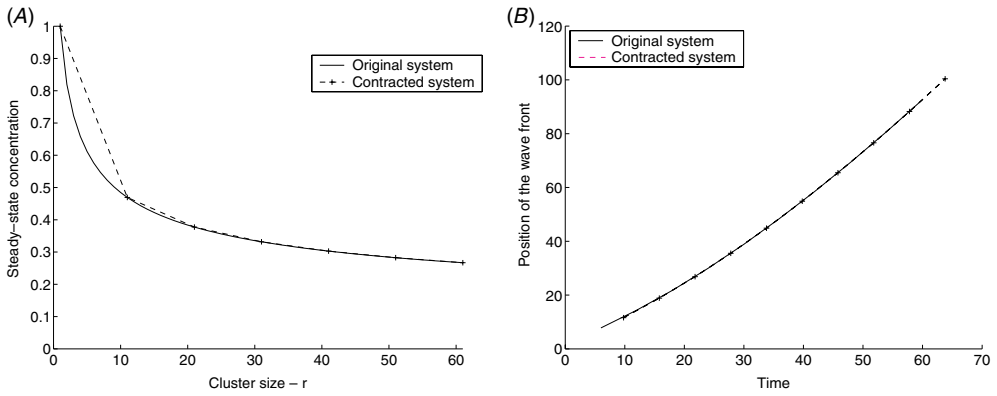

Figure 7. (*A*) Steady-state concentration against cluster size for full and coarse-grained system in the case A(i); $q < p < \frac{1}{2}$ with $a = 1.7, b = 1.4$, $p = 0.2, q = 0.1, \lambda = 10$ and $c_1 = 1$. The results are plotted at large time, $t = 200$, when we expect the systems to have reached their respective steady-state solutions. (*B*) Plot of the position of the erfc function (by determining where the function equates to $\frac{1}{2}$) for the original ($s(t)$) and coarse-grained system ($\Lambda_{\eta(t+3.8)+1.4}$). The positions are found to match exactly.

By assuming the standard leading order form $\Psi(n, t) = H(\eta(t) - n)$ we deduce that

$$\dot{\eta} = \frac{L}{J} a x_1 \lambda^p \eta^p. \tag{56}$$

As previously we require that $\dot{s} = \lambda\dot{\eta}$ and so by comparing equations (28) and (56) we deduce that $A = 1/\lambda$. We show in figure 7 a numerical integration of the system with $a = 1.7, b = 1.4$, $p = 0.2, q = 0.4, c_1 = 1$ and $\lambda = 10$ and compare the position of the wave front in the original and coarse-grained system; these match exactly following a shift of time and cluster size by constants, arising from the fact the above analysis is a leading order result for large r and t.

Furthermore we investigate the width of the erfc function; transforming (55) by $r = z + s(t)$ we render the wave stationary, and find the equation

$$\frac{\partial \Psi}{\partial t} \sim -a x_1 s^{p-1} p z \frac{\partial \Psi}{\partial z} + \frac{a x_1 s^p \lambda}{2} \frac{\partial^2 \Psi}{\partial z^2} \tag{57}$$

the required solution of which is

$$\Psi = \frac{1}{2} \operatorname{erfc}\left(\frac{(r - s(t))\sqrt{1 - 2p}}{\sqrt{2s\lambda}} \right). \tag{58}$$

By comparing this with the result from the original system, given by equation (4.63) in King and Wattis [11], the ratio of the width in the original (w_o) and coarse-grained (w_c) systems is found to be $w_o/w_c = 1/\sqrt{\lambda}$, which is expected from (45) since case A(i) should match with case S(i) in the limit $\theta \longrightarrow \infty$. We note that this is the maximum possible error for the width.

We now consider the fragmentation-dominated regime where the equilibrium solution prevails, to show that the same choice of T_n as given by (36) with $A = 1/\lambda$ also matches the speed of evolution to this state.

3.6. Case F(i): $p < q < \frac{1}{2}$

With $p < q < \frac{1}{2}$ the large-n limit is dominated by the fragmentation term and in this limit equation (36) reduces to

$$T_n \sim \frac{1}{\lambda b^{\lambda-1}(\lambda n)^{(\lambda-1)q}} \tag{59}$$

and we wish to show that this correctly matches the speed of evolution to the equilibrium state also. Using the substitution $c_r = Q_r c_1^r \psi(r,t)$ King and Wattis [11] conclude that ψ converges to unity by a diffusive wave which travels at speed given by (31). It is this speed we wish to reproduce in the coarse-grained system.

Substituting $x_n = Q_{\Lambda_n} x_1^{\Lambda_n} \Psi(n,t)$ into equation (9) and taking the continuum approximation at large n yields

$$\frac{\partial \Psi}{\partial t} \sim -T_n b^\lambda (\lambda n)^{\lambda q} \frac{\partial \Psi}{\partial n}. \tag{60}$$

Hence to leading order Ψ is the Heaviside step function, that is $\Psi(n,t) = H(\eta(t) - n)$, so we obtain

$$\dot{\eta} = T_\eta b^\lambda (\lambda \eta)^{\lambda q}. \tag{61}$$

Requiring that $\lambda \dot{\eta} = \dot{s}$, where $\dot{s} = b s^q$ yields the difference equation

$$b(\lambda \eta)^q = T_\eta b^\lambda (\lambda \eta)^{\lambda q} \tag{62}$$

for T_η. Substitution reveals that the expression for T_n given by (36) solves (62) in the limit $\eta \longrightarrow \infty$ confirming that the solution (59) for T_n does indeed match the speed of evolution between the original and coarse-grained systems. With T_n given by (59) we consider (60) and include the next order terms to give

$$\frac{\partial \Psi}{\partial t} \sim \frac{\lambda b s^q}{2} \frac{\partial^2 \Psi}{\partial z^2} - bq z s^{q-1} \frac{\partial \Psi}{\partial z} \tag{63}$$

where $z = r - s(t)$, which is solved by

$$\Psi = \operatorname{erfc}\left(\frac{(r - s(t))\sqrt{1-2q}}{\sqrt{2\lambda}} \right). \tag{64}$$

By comparison with (30), the ratio of the widths between the original and coarse-grained system is $w_o/w_c = 1/\sqrt{\lambda}$, as expected from considering the limit of $\theta \longrightarrow 0$ of (45), from case E(i).

3.7. Summary

In section 2 the form of T_n was derived to ensure that, in addition to correctly reproducing the equilibrium solution, the coarse-grained system also converges to the correct steady-state solution; and in both cases that the kinetics are also correctly reproduced, by which we mean that the diffusive wave travels at the correct speed. With the rate coefficients $a_r = a r^p$ and $b_r = b r^q$ and an even mesh function it has been shown that the choice $A = 1/\lambda$ satisfies all these. The ratio of the widths of the diffusive wave in the original system and the coarse-grained system have been calculated and differ by at most a factor of $1/\sqrt{\lambda}$, in the limiting cases A(i) and F(i) and for S(i) and E(i) is given by

$$\frac{w_o}{w_c} = \sqrt{\frac{(\theta+1)(\theta^\lambda - 1)}{\lambda(\theta^\lambda + 1)(\theta - 1)}}. \tag{65}$$

The following section considers the complications that arise when the mesh function is n-dependent.

By comparing the large time asymptotic solution of the Lyapunov function in the original and coarse-grained systems we make a further check on the coarse-graining procedure; we assume a uniform mesh function. For the case S ($p = q < 1, \theta > 1$) the system tends to a steady-state solution and in the large-t (and hence large-s) limit we have, to leading order, $c_r(t) = (c_1/r^p)H(r - s(t))$ where $H(\cdot)$ is the Heaviside step function; thus (6) simplifies to

$$V(\{c_r\}) = -c_1 \left(\sum_{r=1}^{s} \left[\frac{\log\theta}{r^{p-1}} + \frac{1 - \log\theta}{r^p} \right] \right) \tag{66}$$

and approximating the summations in the large-s limit by $\sum_{k=1}^{s} k^q \sim s^{q+1}/(q+1)$ where $-1 < q$ yields, to leading order

$$V(\{c_r\}) \sim \frac{-c_1 s^{2-p} \log\theta}{2-p}. \tag{67}$$

Substituting $x_n(t) = \left(x_1 \big/ \Lambda_n^p\right) H(\eta(t) - n)$ into (13) yields

$$V(\{x_n\}) = -\lambda x_1 \left(\sum_{n=1}^{\eta} \left[\frac{\log\theta}{\Lambda_n^{p-1}} + \frac{\log\theta - 1}{\Lambda_n^p} \right] \right). \tag{68}$$

We approximate the summations as above and then assume $\Lambda_n = \lambda n$ in the large-n limit, so that to leading order

$$V(\{x_n\}) \sim -\frac{x_1 (\lambda\eta)^{2-p} \log\theta}{2-p} \tag{69}$$

which is in agreement with (67) since the choice of $A = 1/\lambda$ ensures that $s = \lambda\eta$. We repeat a similar calculation for the case E ($p = q < 1, \theta < 1$). In this case the function V tends to a lower bound, V_∞, as the solution tends to the equilibrium state, by assuming $c_r(t) = \theta^{r-1} c_1 H(r - s(t))/r^p$ and using (6) we obtain

$$V(\{c_r\}) - V_\infty(\{c_r\}) = \sum_{r=s+1}^{\infty} \frac{c_1 \theta^{r-1}}{r^p}. \tag{70}$$

We transform the co-ordinates with $r = s + k$ and take the large-s limit so that

$$V(\{c_r\}) - V_\infty(\{c_r\}) = \frac{c_1\theta^s}{s^p} \sum_{k=1}^{\infty} \frac{\theta^{k-1}}{(1 + k/s)^p} \sim \frac{c_1\theta^s}{s^p} \frac{1}{(1-\theta)}. \tag{71}$$

For the coarse-grained system, with (13) and $x_n(t) = \theta^{\Lambda_n - 1} c_1 H(n - \eta) \big/ \Lambda_n^p$, we find that

$$V(\{x_n\}) - V_\infty(\{x_n\}) = \sum_{n=\eta+1}^{\infty} \frac{\lambda \theta^{\Lambda_n - 1} x_1}{\Lambda_n^p} \tag{72}$$

and first substituting $\lambda_n = \lambda(n-1) + 1$, then transforming the co-ordinates with $n = \eta + k$ and finally taking the large-η limit, yields

$$V(\{x_n\}) - V_\infty(\{x_n\}) = \frac{\lambda x_1 \theta^{\lambda\eta}}{(\lambda\eta)^p} \sum_{k=0}^{\infty} \frac{(\theta^\lambda)^k}{(1 + k/\eta + 1/\lambda\eta)^p} \sim \frac{x_1\theta^{\lambda\eta}}{(\lambda\eta)^p} \frac{\lambda}{(1-\theta^\lambda)}. \tag{73}$$

Comparing (71) and (73) with $s = \lambda\eta$ we note that the time dependence of the two expressions match ($\theta^{s(t)}/s(t)^p$), the scalar multiplier of the coarse-grained system ($\lambda x_1/(1-\theta^\lambda)$) is in error; however, this scalar is correct in the limit $\theta \longrightarrow 1$.

Case A ($1 > p > q$) tends to a steady-state solution and to leading order $c_r(t) = c_1 J H(s(t) - r)/ar^p$. In this case the Lyapunov function (6) is dominated by the latter terms in the summation and so

$$V(\{c_r\}) \sim \frac{-c_1 J}{a} \sum_{r=1}^{s(t)} \frac{(p-q)\log(r!) + r\log\theta}{r^p} \qquad \text{as} \quad t \to \infty. \tag{74}$$

This is approximated using Stirling's formula

$$V(\{c_r\}) \sim \frac{-c_1 J s^{2-p}(p-q)}{a(2-p)} \left(\log s + \frac{\log\theta}{p-q} - 1 - \frac{1}{2-p} \right) \qquad \text{as} \quad t \to \infty. \tag{75}$$

In the coarse-grained system we have $x_n(t) = x_1 J H(\eta(t) - n)/a\Lambda_n^p$ and so (13), with Stirling's formula and $\Lambda_n \sim \lambda n$, becomes

$$V(\{x_n\}) \sim \frac{-x_1 J(\lambda\eta)^{2-p}(p-q)}{a(2-p)} \left(\log(\lambda\eta) + \frac{\log\theta}{p-q} - 1 - \frac{1}{2-p} \right) \tag{76}$$

which, with $\lambda\eta = s$, matches with (75). Finally we consider the case F ($1 > q > p$) which tends to the equilibrium solution according to $c_r(t) = \theta^{r-1} c_1 H(s(t) - r)/r^p$ at leading order, and so

$$V(\{c_r\}) - V_\infty(\{c_r\}) = \sum_{r=s+1}^{\infty} \frac{\theta^{r-1} c_1}{r^p (r!)^{q-p}} \tag{77}$$

which is dominated by the first term, hence

$$V(\{c_r\}) - V_\infty(\{c_r\}) \sim \frac{\theta^{s(t)} c_1}{(s(t)+1)^p ([s(t)+1]!)^{q-p}} \qquad \text{as} \quad t \to \infty. \tag{78}$$

The equivalent calculation for the coarse-grained system yields

$$V(\{x_n\}) - V_\infty(\{x_n\}) = \frac{\lambda x_1 \theta^{\lambda\eta}}{(\lambda\eta+1)^p ([\lambda\eta+1]!)^{q-p}} \tag{79}$$

which with $\lambda\eta = s$ gives the same time dependence as the original system (78) but the multiplicative scalar is different.

4. Size-dependent mesh function

Having analysed the coarse-grained system for an even mesh function we proceed to consider the case when Λ_n is size dependent; hence we allow λ_n to be a general function of n such that Λ_n is monotonically increasing and furthermore we insist that λ_n is also monotonically increasing in the large-n limit; such a choice ensures that the mesh becomes increasing coarse at larger aggregation sizes. We consider the case of size-independent rate coefficients, $a_r = a$ and $b_r = b$, with a constant monomer concentration, and with $\theta > 1$. The solution converges to steady state via a diffusive wave which has a constant speed given by $(ac_1 - b)$ [25]. Directly from (36) we obtain

$$T_n = \frac{A(\theta-1)}{b^{\lambda_n - 1}(\theta^{\lambda_n} - 1)} \tag{80}$$

which ensures that the steady-state solution will be correctly reproduced; it remains to investigate the kinetics of the coarse-grained system.

In the large-n limit we simplify the expression for T_n, as given by (80), to obtain to leading order,

$$T_n \sim \frac{L(\theta-1)}{Jb^{\lambda_n - 1}\theta^{\lambda_n}} \tag{81}$$

since the conditions on Λ_n ensure that $\theta^{-\Lambda_n} \gg \theta^{-\Lambda_{n+1}}$ in the large-n limit when $\theta > 1$. Substituting (81) into the definitions of α and β given by (11) yields

$$\alpha_n = \alpha x_1^{-\lambda_n} \qquad \beta_n = \alpha\theta^{-\lambda_n} \tag{82}$$

where $\alpha = A(ax_1 - b)$. Hence the equation for $\dot{x}_n$ (9) with these rate coefficients becomes $\dot{x}_n = \alpha(x_{n-1} - x_n)$. Assuming that $x_n = x_1\Psi(n, \tau)$, and making a leading order continuum approximation for Ψ gives

$$\frac{\partial\Psi}{\partial\tau} = -\alpha\frac{\partial\Psi}{\partial n}. \tag{83}$$

If we assume that $\Psi(n, t) = H(\eta(t) - n)$ then the speed of the wave is given by $\dot{\eta} = A(ax_1 - b)$, and any choice of A fails to match the speeds of evolution (unless the mesh function is asymptotically n-independent). Since the speed of the diffusive wave in the coarse-grained system is constant, as well as the original system the only case where the speeds can be matched is if the mesh function is also size independent, that is an even mesh; thus with a non-uniform mesh it is not possible to match both the kinetics and the steady-state solution.

4.1. Convergence equilibrium in coarse-grained systems

For a system approaching an equilibrium solution any choice of T_n will allow the equilibrium solution to be correctly reproduced in the coarse-grained system. Thus we can define T_n such that the speed of evolution to the equilibrium solution is correct in the coarse-grained system. This has the obvious possibility that the steady state may no longer be faithfully reproduced. We continue to consider the specific example of $a_r = a, b_r = b$ and now impose $\Lambda_n = n^2$ with $\theta < 1$, the following calculation can be repeated for any mesh function. Calculating the speed of propagation of the diffusive wave yields the difference equation

$$\dot{\eta} = T_{\eta-1}\left(\prod_{k=\Lambda_{\eta-1}+1}^{\Lambda_\eta} b_k\right) - T_\eta\left(\prod_{k=\Lambda_\eta}^{\Lambda_{\eta+1}-1} a_k\right)x_1^{\lambda_\eta} \tag{84}$$

where $\dot{\eta}$ is the speed of the wave front in the coarse-grained system. This is rearranged to give the form

$$\dot{\eta}Q_{\Lambda_\eta}x_1^{\Lambda_\eta} = \left(\prod_{k=0}^{\lambda_{\eta-1}-1} a_{\Lambda_{\eta-1}+k}\right)Q_{\Lambda_{\eta-1}}x_1^{\Lambda_\eta}T_{\eta-1} - \left(\prod_{k=0}^{\lambda_\eta-1} a_{\Lambda_\eta+k}\right)Q_{\Lambda_\eta}x_1^{\Lambda_{\eta+1}}T_\eta. \tag{85}$$

With the reaction rates being considered and since $s = \Lambda_\eta$ we expect $\dot{\eta} = s/2\eta$, thus the above equation simplifies to

$$\frac{(b - ax_1)Q_{\Lambda_\eta}}{2\eta} = Q_{\Lambda_{\eta-1}}a^{\lambda_{\eta-1}}T_{\eta-1} - a^{\lambda_\eta}Q_{\Lambda_\eta}T_\eta. \tag{86}$$

Summing this expression from $i = 2$ to n yields T_n in terms of T_1 which is obtained by summing from $i = 2$ to ∞; hence

$$T_n = \frac{1}{a^{\lambda_n}Q_{\Lambda_n}}\sum_{i=n+1}^{\infty}\frac{(b - ax_1)Q_{\Lambda_i}}{2i} \tag{87}$$

where we have assumed that the summation converges and this condition remains to be proved. This reduces to determining if $\sum_{i=n+1}^{\infty} Q_{\Lambda_n}(b - ax_1)/2n \longrightarrow 0$ as $n \longrightarrow \infty$; this has the

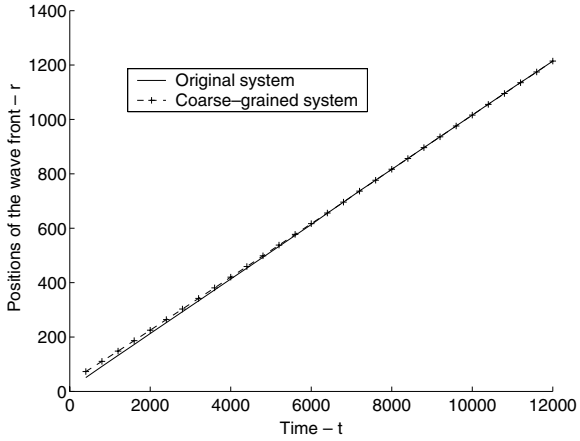

Figure 8. The constant monomer Becker–Döring system is solved with size-independent rate coefficients $a_r = 1.2, b_{r+1} = 1.3$ and also $c_1 = 1$. Dividing the equilibrium solution by the numerical result gives the shape of the wave as an $\frac{1}{2}\mathrm{erfc}((r - (b - ac_1)t)/\sqrt{2(ac_1 + b)t})$, the position of which is defined to be where this function is $\frac{1}{2}$. The system is coarse grained according to $\Lambda_n = n^2$ and the positions compared; these are found to match exactly in the large time limit, with the greatest accuracy being obtained following a shift of -33 applied to the coarse-grained position.

form $\sum_{i=n+1}^{\infty} \theta^{\Lambda_i}/i < \sum_{i=n+1}^{\infty} \theta^i/i$ which obviously converges as $\theta < 1$. For the purposes of numerical calculation the most reliable form of T_n is

$$T_n = \frac{b - ax_1}{2a^{2n+1}} \sum_{i=n+1}^{\infty} \frac{\theta^{i^2-n^2}}{i} \tag{88}$$

which is equivalent to (87). This result is confirmed numerically, with the parameters $a = 1.2, b = 1.3$ and $c_1 = 1$. The positions of the wave front are plotted in figure 8 and with a shift of -33 applied to the coarse-grained system they match exactly in the large time limit. Using the above parameters the strengths and weaknesses of the coarse-grained procedure are summarized by the plots in figure 9. The time-dependent function $\Psi(\psi)$ is plotted for the coarse-grained (original) system in the time range $0 \leqslant t \leqslant 6800$ in steps of 400. The position of the wave in the coarse-grained system is shifted by -33 to match with the original system in the large time limit and these positions are indicated on the plots. From figure 9 we clearly observe that the weakness of the coarse-grained system is that while it retains the characteristic erfc shape, the width of this function is exaggerated; however, the computational saving is massive, in the range plotted, 1200 grid points were required for the original system while the coarse-grained system required only 35, which in CPU time, translates to the original system taking approximately 490 times as long to solve as the coarse-grained system.

5. Spherical cluster growth

Duncan and Soheili [10] have numerically compared various methods for reducing the Becker–Döring equations against solutions of the original system; one method tested was the coarse-graining scheme with $T_n = 1\,\forall n$, which did not compare favourably with other schemes at

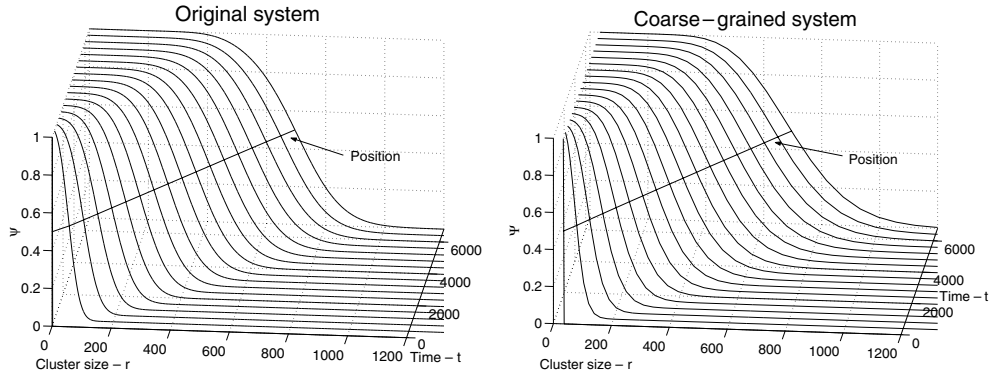

Figure 9. The constant monomer Becker–Döring system is solved with rate coefficient $a_r = 1.2, b_{r+1} = 1.3$ and also $c_1 = 1$. Dividing the numerical solution by the equilibrium solution yields the time-dependent part of the solution, ψ or Ψ for the original or coarse-grained system, respectively. This is plotted for the original and coarse-grained system where a mesh of $\Lambda_n = n^2$ was used, over the time range $0 \leqslant t \leqslant 6800$. While the coarse-grained system faithfully reproduces the position and characteristic shape of the erfc function, the width is exaggerated; however, the computational saving is massive with the original system requiring 1200 grid points, the coarse-grained system requiring only 35.

small times but approached the correct equilibrium solution in the large time limit. In their simulations a constant density system was used with the reaction rate coefficients

$$a_r = 1 \qquad b_{r+1} = \exp(r^{2/3} - (r-1)^{2/3}) \quad \forall r \tag{89}$$

which have physical relevance for the growth of spherical clusters [16]. This gives a partition function $Q_r = \exp(-(r-1)^{2/3})$ with equilibrium solution $c_r = Q_r z^r$ which is monotonically decreasing for $z \leqslant 1$. We consider an approximation to the system with the above reaction rate coefficients initially with a constant monomer condition; then return to a constant density system and use the same choice of T_n as for the constant monomer case and solve numerically to demonstrate that the results have been improved with this choice of T_n. Throughout, the mesh function is assumed to be size independent.

5.1. Constant monomer system

We numerically solve the constant monomer system with reaction rate coefficients given by (89) with parameters $c_1 = 1$ and $\lambda = 5$, where the mesh function is size independent. Using the form of T_n as given by (36) with $A = 1/\lambda$ the steady-state solution of the coarse-grained system matches that of the original system exactly, as shown in figure 10. Furthermore we wish to match the speed of evolution to this state, the speed is matched in the large-r limit and the reaction rate coefficients (89) are approximated by

$$a_r = 1 \qquad b_r \sim 1 + \frac{2}{3r^{1/3}}. \tag{90}$$

We factorize the solution according to $c_r(t) = Q_r c_1^r \psi_r(t)$ and hence find

$$\frac{\partial \psi_r}{\partial t} = b_r \psi_{r-1} - b_r \psi_r - \psi_r + \psi_{r+1} \tag{91}$$

with $c_1 = 1$. In the large-r limit a continuum approximation is valid, yielding

$$\frac{\partial \psi_r}{\partial t} \sim -\frac{2}{3r^{1/3}} \frac{\partial \psi_r}{\partial r} + \frac{\partial^2 \psi_r}{\partial r^2} \tag{92}$$

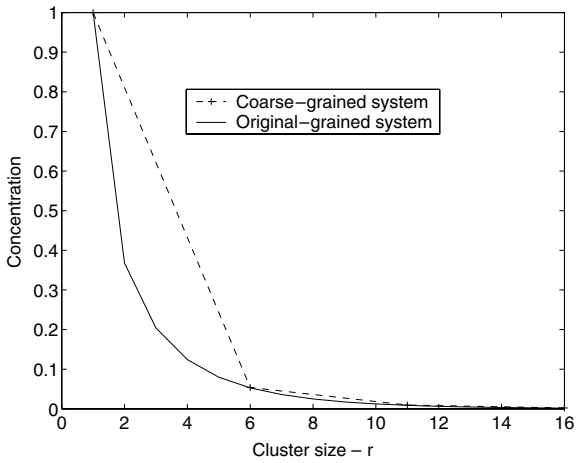

Figure 10. Cluster distribution function approached in the large asymptotic limit of the constant monomer Becker–Döring system, with rate coefficients $a_r = 1$ and $b_{r+1} = \exp(r^{2/3} - (r-1)^{2/3})$ and $c_1 = 1$. The dashed line shows the large time solution for a coarse-grained system with a size independent mesh with $\lambda = 5$.

hence to leading order $\psi = H(r - s(t))$ where $\dot{s} = 2/3s^{1/3}$, which in turn yields the position of the wave front

$$s \sim \left[\tfrac{8}{9}t\right]^{3/4} \qquad \text{as} \quad t \longrightarrow \infty. \tag{93}$$

Transforming the co-ordinates to a frame of reference in which the wave is stationary via $r = z + s(t)$ yields

$$\frac{\partial \psi}{\partial t} \sim \frac{2z}{9s^{4/3}} \frac{\partial \psi}{\partial z} + \frac{\partial^2 \psi}{\partial z^2} \tag{94}$$

and further using s as an internal time variable gives

$$\frac{\partial \psi}{\partial s} \sim \frac{z}{3s} \frac{\partial \psi}{\partial z} + \frac{3s^{1/3}}{2} \frac{\partial^2 \psi}{\partial z^2}. \tag{95}$$

The dominant balance occurs when $z \sim s^{2/3}$, and the required solution is

$$\psi \sim \frac{1}{2} \operatorname{erfc}\left(\frac{r-s}{\sqrt{3}s^{2/3}}\right) \qquad \text{as} \quad t \longrightarrow \infty \qquad \text{with} \quad r - s(t) = \mathcal{O}(s^{2/3}). \tag{96}$$

The system is solved numerically and the position of the wave front plotted in figure 11 alongside the above analytical prediction (93), with a shift of +21 and +70 applied to the position and time of the analytical result, the results are shown to match; the graph is plotted on a log–log scale and the gradient is found to be 3/4 as expected.

Having demonstrated that the form of T_n as given by (36) correctly reproduces the equilibrium solution in the coarse-grained system we further match the speed of evolution to this state with (93). Firstly we factorize the coarse-grained solution with $x_n(t) = x_1^{\Lambda_n} Q_{\Lambda_n} \Psi_n(t)$ and substitute this into (9) to obtain

$$\dot{\Psi}_n = T_{n-1} \left(\prod_{k=\Lambda_{n-1}+1}^{\Lambda_n} b_k \right) (\Psi_{n-1} - \Psi_n) + T_n(\Psi_{n+1} - \Psi_n) \tag{97}$$

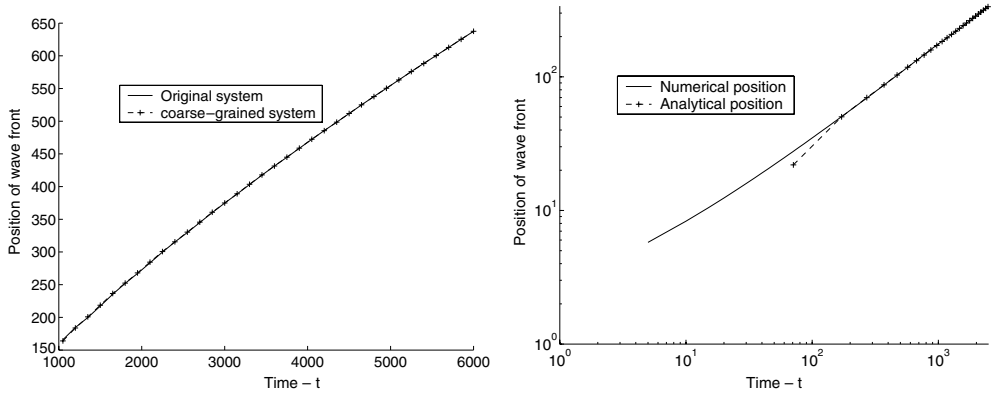

Figure 11. Position of the diffusive wave (where $\Psi = \frac{1}{2}$) against time on both normal and log–log scales, for the constant monomer Becker–Döring system is solved with rate coefficients $a_r = 1$ and $b_{r+1} = \exp(r^{2/3} - (r-1)^{2/3})$. The numerical result is shown to match with the analytic result with a shift of +70 and +21 applied to the time and position, respectively. The results are plotted on a log–log scale and the gradient is $\frac{3}{4}$ as expected.

which, in the large-n limit, where a continuum approximation is valid, yields

$$\frac{\partial \Psi}{\partial t} \sim \frac{\partial \Psi}{\partial n}\left(T_n - T_{n-1}\prod_{k=\Lambda_{n-1}+1}^{\Lambda_n} b_k\right) + \frac{1}{2}\frac{\partial^2 \Psi}{\partial n^2}\left(T_{n-1} + T_n\right). \tag{98}$$

The speed of the wave is governed by the coefficient of the first n derivative, and the large-n limit simplifies this expression. Firstly as $n \longrightarrow \infty$, T_n is approximated by

$$T_n = \frac{A}{\lambda}\left(1 - \frac{\lambda^2 + 4\lambda - 1}{3\lambda(\lambda n)^{1/3}}\right). \tag{99}$$

Secondly we rewrite the product of the fragmentation terms by

$$\prod_{k=\Lambda_{n-1}+1}^{\Lambda_n} b_k \sim 1 + \sum_{\Lambda_{n-1}+1}^{\Lambda_n} \frac{2}{3r^{1/3}} \sim 1 + \frac{2\lambda}{3(\lambda n)^{1/3}} \tag{100}$$

where all the neglected terms are of a lower order of magnitude than those retained. Thus (98) simplifies to

$$\frac{\partial \Psi}{\partial t} \sim -\frac{2A}{3(\lambda n)^{1/3}}\frac{\partial \Psi}{\partial n} + \frac{A}{\lambda}\frac{\partial^2 \Psi}{\partial n^2} \tag{101}$$

and so $\dot{\eta} = 2A/3(\lambda n)^{1/3}$. To match the speed to the original system we insist that $\lambda\dot{\eta} = \dot{s}$ and hence deduce that $A = 1/\lambda$. This result is confirmed numerically in figure 11 where the original and coarse-grained systems are compared on the basis of the position of the wave front; with $\lambda = 10$ and $x_1 = 1$ these are found to match with a shift of -0.1735 applied to the coarse-grained position. Transforming equation (101) to the original co-ordinates (r, t) with $n = r/\lambda$ yields equation (92) with $A = 1/\lambda$ and hence

$$\Psi \sim \frac{1}{2}\operatorname{erfc}\left(\frac{\lambda(n-\eta)}{\sqrt{3}(\lambda\eta)^{2/3}}\right) \tag{102}$$

that is the width of the erfc function in the coarse-grained system will match exactly with the original system.

5.2. Constant density system

An alternative system to the constant monomer scheme discussed above is to insist that the density in the system remains constant, thereby allowing the monomer concentration to vary; defining the density to be $\rho = \sum_{r=1}^{\infty} r c_r$ results in

$$\dot{c}_1 = -J_1 - \sum_{r=1}^{\infty} J_r. \tag{103}$$

Hence the system has been transformed into a more complex nonlinear problem. Obviously numerically solving this system requires that it to be truncated at a finite system size $r_{\max}$. Ball *et al* [2] demonstrate that the behaviour of the truncated system converges to that of the full system in the limit $r_{\max} \longrightarrow \infty$. The behaviour of the infinite system depends on the radius of convergence of the series

$$\rho(z) = \sum_{r=1}^{\infty} r Q_r z^r \tag{104}$$

and for the rate coefficients chosen (89) this has a finite radius of convergence $z_s = 1$, so that $\rho_s = \rho(z_s) = 4.898$ is the critical density, called the density of saturated vapour. If $\rho \leqslant \rho_s$ then the system tends to the equilibrium solution $\bar{c}_r = Q_r \bar{c}_1^r$. However, if $\rho \geqslant \rho_s$ then the solution is more complicated. In the limit $t \longrightarrow \infty$, $c_r \longrightarrow Q_r z_s^r$, and the excess density $\rho - \rho_s$ is swept off to increasingly large cluster sizes as time progresses. This process is extremely slow and is hence described as metastable [16]. The truncated constant density system can also exhibit metastability if the system size $r_{\max}$ and the density ρ are large enough. In contrast to the infinite system, the truncated system eventually reaches an equilibrium solution satisfying $\rho = \sum_{r=1}^{r_{\max}} Q_r \bar{c}_1^r$, where again metastability can be observed if $\bar{c}_1 > z_s = 1$ and $r_{\max}$ is sufficiently large. It is this latter metastable system that is the subject of this section.

5.3. Coarse-grained constant density model

To produce the correct dynamics, the coarse-grained system needs to be carefully altered to allow the monomer concentration to vary. Using equations (7)–(9) and the coarse-grained density (15) we are able to define an expression for $\dot{x}_1$; which with a uniform mesh leads to

$$\dot{x}_1 = -\lambda L_1 - \sum_{n=1}^{\infty} \lambda^2 L_n \tag{105}$$

and the system is truncated by defining $L_n = 0$ for $n \geqslant n_{\max}$, where $\Lambda_{n_{\max}} = r_{\max}$.

Previously Duncan and Soheili [10] used the constant density model presented above to assess various methods of reducing the dimensionality of the Becker–Döring scheme and it was found that the coarse-grained system performed poorly when compared with other methods. Previously it was assumed that $T_n = 1 \, \forall n$ which we shall refer to as case I; here we show that using the formula (36) for T_n, derived for the constant monomer system, increases the accuracy of the coarse-grained constant density system considerably. The formula for T_n depends on the monomer concentration and there are two ways to estimate this in the case where we allow x_1 to vary with time. Either the monomer concentration used in the formula for T_n is set to the equilibrium monomer concentration, that is $x_1 = \bar{x}_1$ which we shall refer to as case II; or T_n is re-evaluated at each time step with the current value of the monomer concentration, that is replacing x_1 in (36) with $x_1(t)$, which we shall refer to as case III. We note that in each of these cases the mesh function remains constant over time and the formula for T_n remains as given by (36), and the three different cases evaluate the parameter x_1

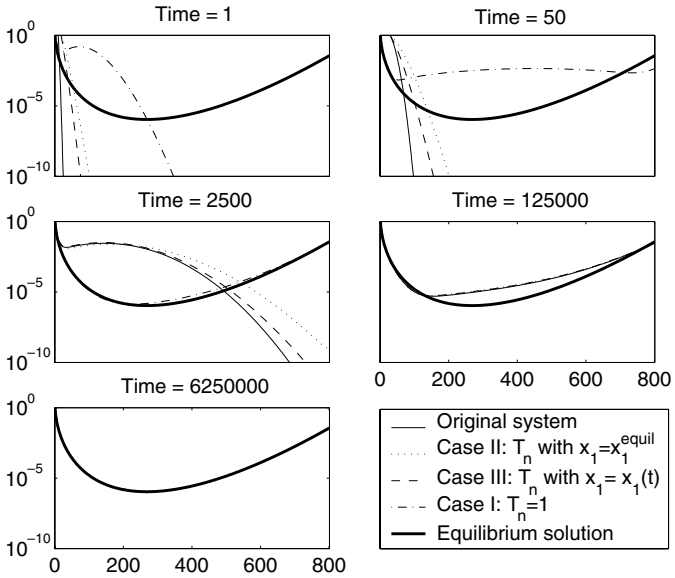

Figure 12. The log of the concentration profile is plotted against size at successive times for the constant density Becker–Döring system solved with rate coefficient $a_r = 1$ and $b_{r+1} = \exp(r^{2/3} - (r-1)^{2/3})$ with $\bar{c}_1 = 1.109$ and $n_{\max} = 801$. The original system is contracted with $\lambda = 10$ with either case I, where $T_n = 1$; case II, where T_n with $x_1 = \bar{x}_1$; or finally, case III, where $T_n(t)$ with $x_1 = x_1(t)$ in the formula for T_n. Relatively rapidly we observe that the mass aggregates to the maximum cluster size, after which the system relaxes to equilibrium over a longer timescale. We note that dynamics for case I are greatly accelerated while case III appears to be a more accurate approximation to the original system than case II.

in (36) either by setting it at unity, or by the equilibrium monomer concentration or the current monomer concentration. In the first two cases the quantities T_n are time independent, in the third they vary with time, but in a predetermined way given by (36), there is no *a posteriori* fitting of data. The system to be investigated has a density above the critical density ρ_s and so metastable behaviour is expected and hence there is a need to approximate the system well to allow the large time behaviour to be investigated.

Firstly we define a measure of the relative error of each approximation. For the examples given below the original system has been solved to give the exact solution $c_r^e(t)$ and thus the relative error of a coarse-grained system is defined to be

$$E(t) = \frac{\left|c_1^e(t) - x_1(t)\right| + \sum_{n=2}^{n_{\max}} \lambda\Lambda_n \left|c_{\Lambda_n}^e(t) - x_n(t)\right|}{\rho}. \tag{106}$$

This weighted norm ensures that the error is measured over the number of monomers per unit volume rather than clusters per unit volume. Using this error estimate the three coarse-grained systems described above are compared.

We numerically investigate the general dynamics for the various systems, a system size of $r_{\max} = 801$ for the original system was chosen, and with $\bar{c}_1 = 1.109$ results in a density $\rho = 944.532$. This was contracted with $\lambda = 10$ and the concentration profile is plotted at a sequence of times in figure 12 with the initial condition being monodisperse, that is with all the mass in monomeric form. For all systems there is a relatively rapid aggregation of mass to the largest cluster size, spreading the mass across the entire range of available cluster

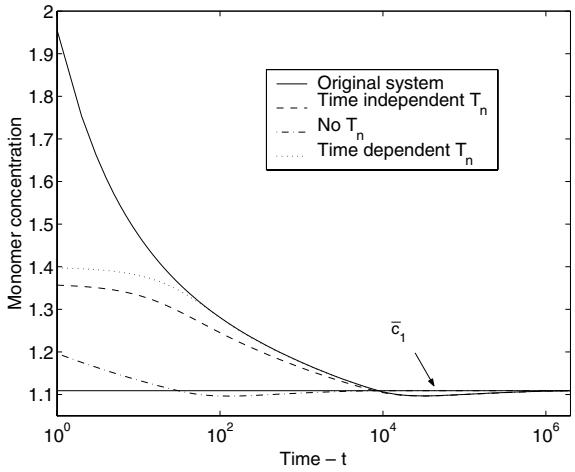

Figure 13. The constant density Becker–Döring system is solved with rate coefficient $a_r = 1$ and $b_{r+1} = \exp(r^{2/3} - (r-1)^{2/3})$ with $\bar{c}_1 = 1.109$ and $n_{\max} = 801$. The original system is contracted with $\lambda = 10$ with either case I where $T_n = 1$; case II where T_n with $x_1 = \bar{x}_1$; or finally, case III, where $T_n(t)$ with $x_1 = x_1(t)$ in the formula for T_n.

sizes. Following this is a relatively slow phase of dynamics over which the system converges to equilibrium solution, typically the mid-range clusters tend to the equilibrium solution from above, while at the extremes small and large clusters tend to the equilibrium solution from below. Case I clearly evolves faster than the other systems, while case III is a more accurate approximation to the original system than case II. To highlight the complex nature of the system in the constant density case we plot the evolution of the monomer concentration for each system, as shown in figure 13. Over a relatively fast timescale the monomer concentration drops below its equilibrium concentration and only over the final timescale does it converge to $\bar{c}_1$. For case III the solution is almost exact for $t > 10^2$, whereas case II is accurate only in the time range $t > 10^4$.

For the contracted systems the initial configuration of concentrations is $x_1 = \rho$, $x_r = 0$ for $r \geqslant 2$. However, since the contracted system represents a group of clusters by one size using this method will introduce discrepancies in the final equilibrium state. Alternatively we use a slightly different density in the coarse-grained system such that $\bar{x}_1 = \bar{c}_1$ and $\bar{x}_n = \bar{c}_{\Lambda_n}$ and then use equation (15) to determine the coarse-grained density which may differ slightly from (104); this method will be used for the remainder of this paper. This has particular significance when calculating the error estimates, since, rather than tending to a non-zero limit the error will tend to zero as $t \longrightarrow \infty$ since in this limit the coarse-grained system exactly reproduces the equilibrium solution.

Cases I, II and III are now compared on the basis of the error estimate given by (106). The error is plotted over time for the three cases in figure 14. All three cases have the characteristic error behaviour of a fast initial rise followed by an exponential decay to zero as all the systems eventually converge to the equilibrium solution. As expected for case I, with $T_n = 1$, the error is large as the dynamics in the coarse-grained system is too fast and the system reaches equilibrium while the original system is still evolving. Case II provides a better approximation with the error being smaller than that of case I at all times but the additional time-dependent information in case III ensures that this is the best approximation.

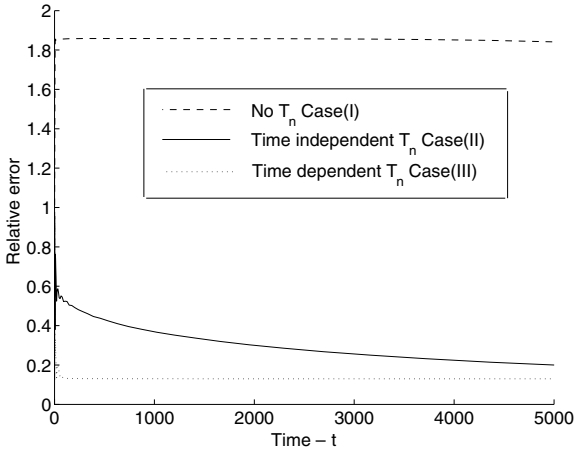

Figure 14. The constant density Becker–Döring system is solved with rate coefficient $a_r = 1$ and $b_{r+1} = \exp(r^{2/3} - (r-1)^{2/3})$ with $\bar{c}_1 = 1.109$ and $n_{\max} = 801$. The original system is contracted with $\lambda = 10$ with either case I, where $T_n = 1$; case II where T_n with $x_1 = \bar{x}_1$; or finally, case III where $T_n(t)$ with $x_1 = x_1(t)$ in the formula for T_n. The relative error of a coarse-grained system is defined by equation (106). In all cases there is an initial rise in the error followed by exponential decay to zero. Case I has the largest error, while case II provides a better approximation. However, case III clearly gives the best representation of the original system.

6. Conclusions

The Becker–Döring model is a microscopic model of nucleation. As such it uses a vast number of ordinary differential equations, one for each possible cluster size in the system and this hinders the numerical, as well as the analytic, attempts at solution; thus there is a need to approximate these equations by a system with a lower dimensionality. One such possibility is the coarse-grained approximation first introduced by Coveney and Wattis [8, 21]; where groups of clusters are represented by a single concentration, a mesh function is defined which gives the cluster groupings with the monomer concentration remaining unapproximated due to its unique nature within the Becker–Döring model. If the mesh function is size independent then each group of λ consecutively sized clusters are gathered together and so the coarse graining is even throughout the system. By using a size-dependent mesh function it is possible to accurately model small clusters, while making an increasingly coarse approximation for the concentrations of larger cluster sizes. In addition to aiding the numerical simulation of the system, the coarse-graining approximation has been used successfully to permit an analytical approach which otherwise would have been hindered by the number of equations.

Previously the coarse-grained reaction rates have been such that the evolution of the system has reproduced the original system but the timescale over which these dynamics occur has not been preserved. Duncan and Soheili [10] used a specific set of reaction rate coefficients applicable to spherical cluster growth to compare the accuracy of various approximations to a constant mass Becker–Döring model, and due to the error in timescale the coarse-grained system performed relatively poorly. The timescale problem was investigated in a simple example by Wattis and King [25] where a temporal rescaling was introduced to correct the timescales. In this paper we have generalized this approximation by multiplying the coarse-grained reaction rates by a size-dependent function T_n such that both the steady-state

solution and the equilibrium solution are preserved (previous work thus corresponds to the case $T_n = 1\ \forall n$). We have derived the form of T_n for the constant monomer Becker–Döring system so that the steady-state solution, in addition to the equilibrium solution, is reproduced correctly as well as matching the speed of convergence to these states. We can expect accurate results from the coarse-graining procedure when J_r and c_r are slowly varying in r which relies upon a_r and b_r to be slowly varying. For algebraic power laws $a_r = ar^p$ and $b_r = br^q$ these conditions are met when r is large, but not when r is close to unity, this explains the poor accuracy at very small times in figure 13. The condition of slow variation in r is also required to take a continuum limit, necessary to analyse the kinetics; thus where we see good agreement between asymptotic results and numerics we also see good agreement between coarse-grained numerics and numerical simulation of the full system; for example, in figure 4, where we get unexpectedly good agreement even at relatively small times. In the examples analysed in this paper we see that the leading order terms in the continuum expansion of the coarse-grained system are identical to the continuum expansion of the full system. Thus the leading order solution of the coarse-grained system will be a good approximation of the full system when the continuum limit is valid.

King and Wattis [11] report on the analytical solution for the case of power law rate coefficients $a_r = ar^p, b_{r+1} = br^q$ (again in the constant monomer Becker–Döring system) and this example was used to demonstrate the accuracy of our generalized coarse-graining procedure. Various parameter regimes were investigated and in each case T_n was derived to match the equilibrium and steady-state solutions. In several examples, the time-dependent part of the solution has an erfc form and the chosen T_n matched the position and shape of this function exactly. The width of the erfc function was in error and the ratio of the original to the coarse-grained widths was found; having a maximum of $1/\sqrt{\lambda}$ in either the aggregation or fragmentation dominated regime, see equation (65) for details. For the borderline case $p = q < \frac{1}{2}, \theta = 1$ the speed of the wave is zero; in this case the widths are found to match exactly.

The n-dependence of T_n has been fully determined for all possible rates a_r and b_{r+1}; this leaves the parameter A undetermined and this corresponds to matching the timescales over which the kinetics occur. In all examples $A = 1/\lambda$ has been derived via detailed asymptotic analysis of the large time solution. Here we briefly show an alternative derivation using the density ρ (104). Firstly we consider the case S(i), $p = q < \frac{1}{2}$ and $\theta > 1$, where the contracted system tends to the steady-state solution $x_n^{sss} = x_1 \big/ \Lambda_n^p$. Assuming a uniform mesh, to leading order Ψ is the Heaviside function located at η; hence, $\rho \sim \sum_{n=1}^{\eta} \lambda \Lambda_n x_n^{sss}$ and the summation can be approximated in the large time, and hence large η, limit to give

$$\rho \sim \frac{\lambda^2 \eta^{2-p} x_1}{\lambda^p (2-p)} \quad \Rightarrow \quad \dot{\rho} \sim \frac{\dot{\eta} \lambda^2 \eta^{1-p} x_1}{\lambda^p} \tag{107}$$

where $\Lambda_n \sim n\lambda$. In contrast we differentiate (104) directly to yield

$$\dot{\rho} = \sum_{n=1}^{\eta} \lambda \Lambda_n \dot{x}_n \quad \Rightarrow \quad \dot{\rho} \sim \lambda^2 \eta L. \tag{108}$$

The constant flux in the system can be obtained from the definitions (11) and (36), namely $L = Ab(\theta - 1)$. Direct comparison of the two expressions for $\dot{\rho}$, (107) and (108), yields

$$\dot{\eta} \sim Ab(\theta - 1)(\lambda \eta)^p \tag{109}$$

which is in agreement with (42) provided $A = 1/\lambda$ as previously. For the case A(i), that is $q < p < \frac{1}{2}$, from equation (25) we find $x_r^{sss} \sim J/(b\theta(\lambda n)^p)$ in the limit $n \longrightarrow \infty$ and with

this expression the density (104) becomes $\rho \sim \lambda\big(\sum_{n=1}^{\eta}(\lambda n)^{(1-p)}J/(b\theta)\big)$. In the large-$\eta$ limit the sum is approximated and differentiated to yield

$$\dot{\rho} \sim \frac{\dot{\eta}\lambda^{2-p}\eta^{1-p}J}{b\theta}. \tag{110}$$

Comparing this expression to (108) with $L = AJ$ yields

$$\dot{\eta} = b\theta(\lambda\eta)^{p} \tag{111}$$

which is in agreement with (56) and hence $A = 1/\lambda$ as previously. Further confirmation of $A = 1/\lambda$ was found by comparing the Lyapunov functions between the original (6) and coarse-grained (13) systems. For cases S(i) and A(i) these were found to match exactly when $A = 1/\lambda$, as this implies that $s = \lambda\eta$. In cases E(i) and A(i) the time dependence of $V - V_{\infty}$ matched; however, the coarse-grained expression was in error by a constant multiplier. For case E(i), this error is eliminated in the limit $\theta \longrightarrow 1$ which we note is also the limit when the coarse-grained system correctly predicts the width of the diffusive wave.

For a size-independent mesh function we derived the form of T_n, in terms of general rate coefficients (36), such that the steady-state solutions and speed of evolution are matched. In the case of a size-dependent mesh function it is not possible to match the speed and the steady-state solution; instead T_n was determined in an instructive example by matching the speed of evolution to the equilibrium state. The power of the coarse-graining procedure was also demonstrated in this example where the original system had 1200 equations while the coarse-grained system had only 35, reducing the computation time by a factor of 490. Thus for cases where the steady-state solutions are not relevant any mesh function can be chosen so that the correct T_n results in the speed of convergence to the equilibrium solution being matched.

The final section dealt with the rate coefficients used by Duncan *et al* [10], namely $a_r = 1, b_{r+1} = \exp(r^{2/3} - (r-1)^{2/3})$. First we considered the constant monomer formulation of the system, the time-dependent part of the solution was derived, equation (96), with position given by $s \sim (8t/9)^{3/4}$. Using the general formula for T_n (36) in the coarse-grained system the steady-state solution and the speed of the erfc function were shown to match exactly with the original system. Secondly we considered the constant density formulation of this system, that analysed by Duncan and Soheili [10] who had solved the original system and a coarse-grained system with $T_n = 1$. Defining an error function allowed the performance of three coarse-grained systems to be assessed by comparison with the original solution. The best approximation came from using T_n from the general formula (36) derived previously for the constant monomer system, but using $x_1 = x_1(t)$ so that T_n must be calculated at every timestep, this makes the system computationally more intensive, but only slightly so, and still provides a vast saving over a numerical solution of the full system. In this case the timescales were preserved as well as the final equilibrium solution, yielding a huge improvement on the previous case when $T_n = 1$ (see figure 14).

With the general formula for T_n (36) future coarse-graining approximations with uniform mesh functions can be made much more accurate, preserving not only the steady-state solutions but also the timescales of the dynamics. This will allow otherwise unfeasible systems to be numerically approximated without introducing prohibitive errors and since the dynamics on the long timescales is properly reproduced, this method is excellent for investigating metastable systems. The models analysed in section 3 showed that the coarse-graining procedure works on systems which approach an equilibrium or steady-state distribution of cluster sizes. Other types of rate coefficient, however, allow clusters to grow to arbitrarily large sizes. The classic example of this is the Lifshitz–Slyozov theory [14] for the late stages of droplet nucleation in the presence of monomers. This can be modelled by the Becker–Döring system which

has metastable behaviour in the large-time limit, a phenomenon which has been analysed by Ball *et al* [2] and Penrose [16]. The connections between these two theories have been a topic of much recent activity, most notably by Niethammer [15], Penrose [17] and Velazquez [20]. Whilst we have not tackled exactly the Lifshitz–Slyozov problem, the example studied in section 5 shows some of the same phenomena: in the infinite system there is a maximum density which the system can support at equilibrium, and when the system is initiated with a greater density, the excess mass aggregates into increasingly large clusters. In figure 12, at times 1, 50, 2500 one can see such a distribution of clusters forming and moving to larger cluster sizes. However, the truncation used a density preserving boundary condition at the largest cluster size, so this excess mass is, at later times, seen to build up at the larger sizes. The accuracy seen at intermediate times shows that the coarse-graining method is suitable for studying the form of the cluster size distribution function as arbitrarily large clusters grow. The only restriction being that the size of the mesh function used should be fine enough that the distribution of growing clusters is broader than the mesh size.

Acknowledgment

Colin Bolton is supported by an EPSRC Research Studentship.

References

[1] Ball J M and Carr J 1988 *Proc. Roy. Soc. Edinburgh* A **108** 109
[2] Ball J M, Carr J and Penrose O 1986 *Commun. Math. Phys.* **104** 657
[3] Becker R and Döring W 1935 *Ann. Phys., Lpz* **24** 719
[4] Blackman J A and Marshall A 1994 *J. Phys. A: Math. Gen.* **27** 725
[5] Brilliantov N V and Krapivsky P L 1991 *J. Phys. A: Math. Gen.* **24** 4787
[6] Carr J, Duncan D B and Walshaw C H 1995 *IMAJNA* **15** 505
[7] Carr J and Dunwell R M 1999 *Proc. Edinburgh Math. Soc.* **42** 415
[8] Coveney P V and Wattis J A D 1996 *Proc. R. Soc.* A **452** 2079
[9] Coveney P V and Wattis J A D 1998 *J. Chem. Soc., Faraday Trans.* **94** 233
[10] Duncan D B and Soheili A R 2001 *Appl. Num. Math.* **37** 1
[11] King J R and Wattis J A D 2002 *J. Phys. A: Math. Gen.* **35** 1357
[12] Krapivsky P L 1995 *Phys. Rev.* E **52** 3455
[13] Krapivsky P L and Redner S 1996 *Phys. Rev.* E **54** 3553
[14] Lifshitz I M and Slyozov V V 1961 *J. Phys. Chem. Solids* **19** 35
[15] Niethammer B 2003 *J. Nonlinear Sci.* **13** 115
[16] Penrose O 1989 *Commun. Math. Phys.* **124** 515
[17] Penrose O 1997 *J. Stat. Phys.* **89** 305
[18] Penrose O and Lebowitz J L 1976 *Studies in Statistical Mechanics VII:Fluctuation Phenomena* (Amsterdam: North Holland)
[19] von Smoluchowski M 1916 *Physick Z* **17** 557
[20] Velazquez J J L 1998 *J. Stat. Phys.* **92** 195
[21] Wattis J A D and Coveney P V 1997 *J. Chem. Phys.* **106** 9122
[22] Wattis J A D and Coveney P V 1999 *J. Phys. Chem.* B **103** 4231
[23] Wattis J A D and Coveney P V 2001 *J. Phys. A: Math. Gen.* **34** 8679
[24] Wattis J A D and Coveney P V 2001 *J. Phys. A: Math. Gen.* **34** 8697
[25] Wattis J A D and King J R 1998 *J. Phys. A: Math. Gen.* **31** 7169